Bimetallic alloy based catalyst design for aerobic oxidation of 5-hydroxymethyl-furfural

Yichao Jin

Master of Philosophy

School of Chemistry and Physics

Science Faculty

Queensland University of Technology

2021

Keywords

alloy nanoparticles • HMF oxidation • low temperature • product selectivity • reaction pathway

Abstract

Controlling product selectivity of cascade reaction is as important as improving efficiency in chemical synthesis. Selective oxidation of 5-hydroxymethyl-furfural (HMF) with O_2 over a bimetallic alloy based catalyst to yield 2,5-furandicarboxylic acid (FDCA) is a cascade reaction comprising of several reaction steps. Incomplete oxidation and over oxidation of reactant molecule or intermediate compounds result in different by-products and decrease the selectivity of the target product. In this study, AgPd alloy nanoparticles (NPs) on CeO_2 nanofibre support were prepared and applied as catalysts to HMF oxidation reaction at mild reaction conditions. The product selectivity of the HMF oxidation over the catalyst with Ag:Pd ratio of 1:1, can be switched simply by reaction temperature change. An excellent FDCA (cascade end product) yield can be achieved at 20 °C, while 5-hydroxymethyl-2-furan carboxylic acid (HMFCA, an intermediate) is obtained as the main product at 80 °C. This finding demonstrated that the final oxidation product, FDCA, favours a low reaction temperature on the alloy catalyst surface. The surface Pd sites catalyse both the oxidation of HMF and the formation of by-products, depending on the site size and reaction temperature. The configuration of small Pd clusters segregated by small Ag clusters on the surface of spherical alloy NPs significantly accelerates the oxidation of both alcohol group to carbonyl group and carbonyl group to carboxyl groups at 20 °C without the formation of large molecule. The further heating drives the side reactions to form undesired by-products (large compounds) at 80 °C, and these by-products impede the reaction at HMFCA oxidation step. The surface configuration of the alloys and reaction temperature can be optimised to selectively catalyse the oxidation of the two functional groups.

Table of Contents

List of Figures

List of Tables

List of Abbreviations

HMF	5-hydroxymethyl-furfural
HMFCA	5-hydroxymethyl-2-furan carboxylic acid
FFCA	5-formyl-2-furancarboxylic acid
DFF	2,5-diformylfuran
FDCA	2,5-furandicarboxylic acid
TPA	terephthalic acid
PEF	polyethylene 2,5-furandicarboxylate
PET	polyethylene terephthalate
DHMF	2,5-dihydroxymethylfuran
FDCDCl	2,5-furandicarboxylic dichloride
Equiv	equivalent
NOs	nanooctahedrons
NCs	nanocubes
NPs	nanoparticles
LC-MS	Liquid chromatography-mass spectrometry
TEM	Transmission electron microscopy
XPS	X-ray photoelectron spectroscopy
XRD	X-ray crystallography
EDS	Energy dispersive X-ray spectroscopy
HT	hydrotalcite

Statement of Original Authorship

The work contained in this thesis has not been previously submitted to meet requirements for an award at this or any other higher education institution. To the best of my knowledge and belief, the thesis contains no material previously published or written by another person except where due reference is made.

Signature: QUT Verified Signature

Date: 26/03/2021

Acknowledgements

We gratefully acknowledge financial support from Australian Research Council (ARC DP150102110, ARC DE190101450).

Chapter 1: Introduction

1.1 BACKGROUND

Due to the worldwide increase in the consumption of fuels and chemicals, the chemical industry relies heavily on consuming fossil fuel-derived petrochemicals to produce these fuels and chemicals (Gallezot, 2012). However, these resources are non-sustainable and cause adverse effects on the environment (Goswami et al., 2016). Therefore, exploring efficient processes for the conversion of sustainable resources to fuels and chemicals is of great significance for the development of chemical industry (Corma et al., 2007). Biomass is considered as one of the potential renewable resources to generate fuels and chemicals due to its abundant production with 170 billion metric tons per year (Gallezot, 2012). Furthermore, biomass also plays an important role in carbon balance due to its availability as an organic carbon resource (Morais et al., 2015).

Recently, many researchers have focused on developing new methods to achieve the synthesis of valuable chemicals and fuels from biomass (Corma et al., 2007; Alonso et al., 2010; Hanson et al., 2015; Addepally and Thulluri, 2015; De Clercq et al., 2017; Wang and Wang, 2019). Among them, oxidation of biomass or biomass-based chemicals to valuable chemicals has attracted considerable attention. 5-hydroxymethyl-furfural (HMF), a chemical drived from sugar and cellulose, is one of the most useful platform molecules (Zhao et al., 2007; Li et al., 2011; Kang et al., 2019). As shown in Figure 1.1, selective oxidation of HMF can produce a series of valuable chemicals such as FDCA, DFF, HMFCA and FFCA. Among these chemicals, FDCA is one of the most important platform chemicals (Werpy et al., 2004), which is a monomer in the production of polymers (Jacquel et al., 2015; Rajendran et al., 2015 and Wilsens et al., 2015). The production of polyethylene 2,5-furandicarboxylate (PEF) from FDCA represents a key application in this regard since PEF is a degradable bio-based polymer from renewable raw materials and is more thermally stable compared with its analogue TPA-based PET (Van Nguyen et al., 2016; Zhu et al., 2016). FDCA can also be applied in organic synthetic processes including the synthesis of succinic acid and 2,5-dihydroxymethyl tetrahydrofuran, which are precious chemicals themselves (Zhang and Deng, 2015).

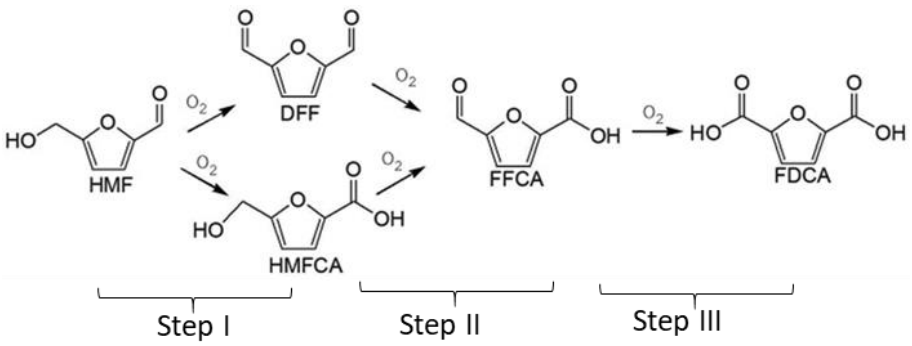

Figure 1. 1 Scheme of selective oxidation of HMF. The oxidation involves three steps (Delidovich et al., 2016).

1.2 THE RESEARCH GAP

The synthesis of FDCA from HMF involves electrocatalytic, biocatalytic and thermal catalytic methods. Compared with electrocatalytic and biocatalytic methods, conventional thermal catalytic oxidation of HMF has several advantages such as higher selectivity to FDCA and the relative ease of scaling up the process to industrial levels (Zhang and Deng, 2015; Sajid et al., 2018). There are still opportunities to achieve high FDCA yield by developing new catalyst and optimizing reaction conditions. Therefore, most researchers have focused on this method. Considerable progress has been achieved in synthesis of FDCA from HMF over various metal supported heterogeneous catalysts such as Au, Pt, Pd, Ru or their alloys in the presence of bases (Sankar et al., 2012). However, almost all catalytic pathways require a high reaction temperature or high O_2 pressure. These reaction conditions certainly require a large amount of energy consumption, which can promote the yield of undesired by-products and cause a safety concern. Therefore, developing novel catalysts for oxidation of HMF under mild conditions is of great importance for the industrial production of FDCA.

1.3 AIMS OF THE PROJECT

In recent years, alloy catalysts has been shown to exhibit distinctly different product selectivity from the catalysts of the single component metal in several systems (Sarina, et al. 2013, Xiao et al. 2016, Peiris et al. 2019). Inspired by the experience, this project aims to develop bimetallic alloy nanoparticles (NPs) catalysts that can harness their structural synergy to catalyze oxidation reactions and significantly improve the reaction efficiency and product selectivity. Literature shows that Ag

catalyst exhibits efficient and high selective oxidation of HMF to HMFCA in basic conditions. However, Ag based catalysts cannot catalyze the oxidation of the alcohol side-chain of HMFCA to aldehyde side-chain of FFCA. Pd catalyst was able to catalyze the oxidation of the alcohol side-chain of HMFCA to aldehyde side-chain of FFCA. However, the catalytic process required elevated temperature and the reaction rate was low (Zhang et al., 2015, An et al., 2019). Ag and Pd atoms have similar size, are infinitely miscible, and both exist as face-centred cubic crystals in the alloy. Hence, it should be feasible to tune the surface configuration of AgPd alloy particles to regulate the reaction rate and pathway. There has been no report yet on AgPd alloy catalyst used for the oxidation of HMF. This study will explore the possibility of Ag based catalysts for the selective oxidation of HMF to FDCA and investigate the possibility of selective oxidation of HMF to FDCA at room temperature and pressure. The knowledge obtained in this study may inspire the design of efficient catalysts for application to selective oxidation of different functional groups in many different reactants.

1.4 RESEARCH OBJECTIVES

To achieve the optimum catalytic performance of the alloy catalyst for selective oxidation of HMF to FDCA, this project will :

(1) Prepare various AgPd alloy catalysts supported on different metal oxide materials and investigate their catalytic activity. The alloy catalyst is prepared via an impregnation–reduction procedure using $NaBH_4$ as the reducing agent. CeO_2 nanofibre is selected as the supporting material for the alloy, as the fibril support is not only good for the diffusion of reactant and product but also strongly binds noble metal NPs and adsorbs O_2 (Huang et al., 2005; Montini et al., 2016; Lei et al., 2020).

(2) Explore the influence of various reaction parameters like pH, reaction temperature, and reaction atmosphere on the selectivity of FDCA to achieve the catalytic process under mild reaction conditions with high TON.

(3) Explore the mechanism of the oxidation of HMF in the AgPd catalytic system, with regard to:

(a) Kinetic studies on the conversion of HMF to FDCA over AgPd catalysts with various Ag:Pd ratio were conducted to confirm the reaction pathway of this catalytic process.

(b) The oxidation of various intermediates as substrates during the oxidation of HMF using AgPd, Ag and Pd catalyst were explored, respectively to confirm the active sites for each oxidation step on AgPd alloy catalyst

(c) The effect of the surface configuration of the alloys were studied through TEM analysis and DFT calculation.

(d) Investigate the influence of the composition of AgPd alloy with different Ag:Pd ratio ranged from 1:5 to 5:1.

(4) Examine the catalyst deactivation and reusability of AgPd catalysts for the oxidation of HMF to FDCA will be examined and the spent catalyst.

Chapter 2: Literature Review

2.1 5-HYDROXYMETHYL-FURFURAL (HMF)

HMF, a common dehydration product of hexose carbohydrates, is listed as top 10+4 biobased chemicals by US Department of Energy (Werpy et al., 2004) due to its high utility in the synthesis of many valuable fuels and chemicals as shown in Figure 2.1. For example, 2,5-dihydroxymethylfuran (DHMF) can be obtained by selective hydrogenation of HMF (Román-Leshkov et al., 2007; Verevkin et al., 2009; Chatterjee et al., 2014; Elangovan et al., 2016). while the selective oxidation of HMF can generate FDCA (Delidovich et al., 2016).

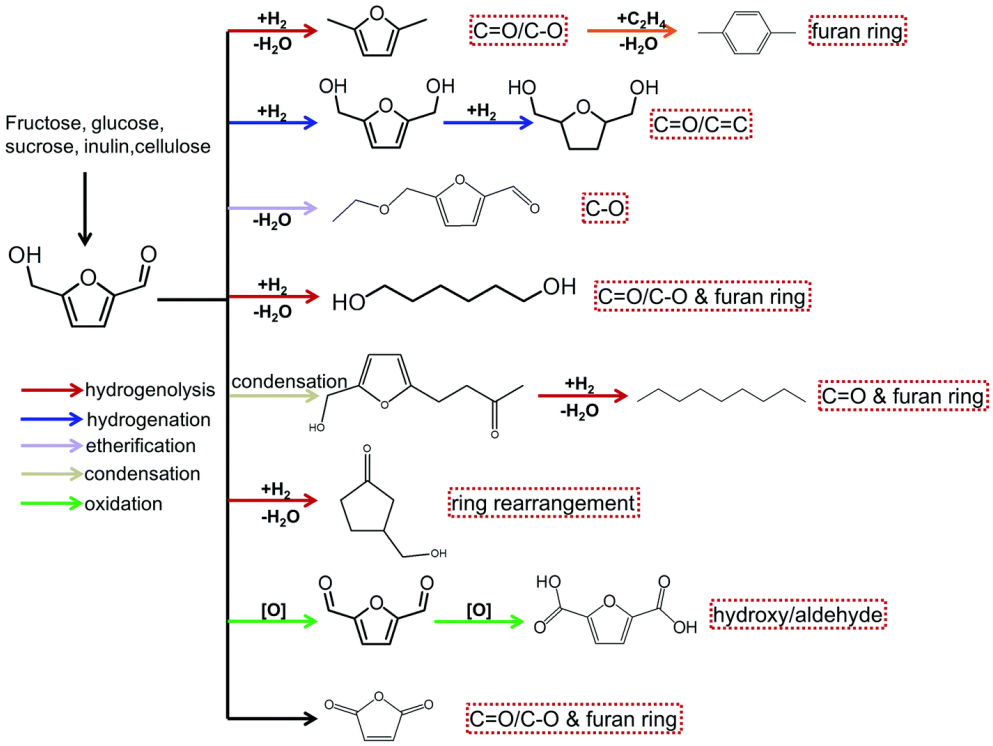

Figure 2.1 Catalytic conversion of HMF into various valuable products (Kong et al., 2018).

The synthesis of HMF has a long history and it can be generated by consecutive dehydration of hexoses. As shown in Figure 2.2, Anet (1964) reported a possible pathway of dehydration of hexoses to HMF. Following the effort of Anet, more intermediates were identified via different hexoses to obtain HMF, which provide various transformation pathways for the synthesis HMF (Moreau et al., 1996 and

Jadhav et al., 2011). Recently, the conversion of glucose and fructose into HMF has become an emerging pathway due to the cheap and rich feedstock in food (Zirbes et al., 2013). However, the side-reactions that generate by-products, such as levulinic acid and formic acid impede scaling-up the process to industrial level (Caes et al., 2015).

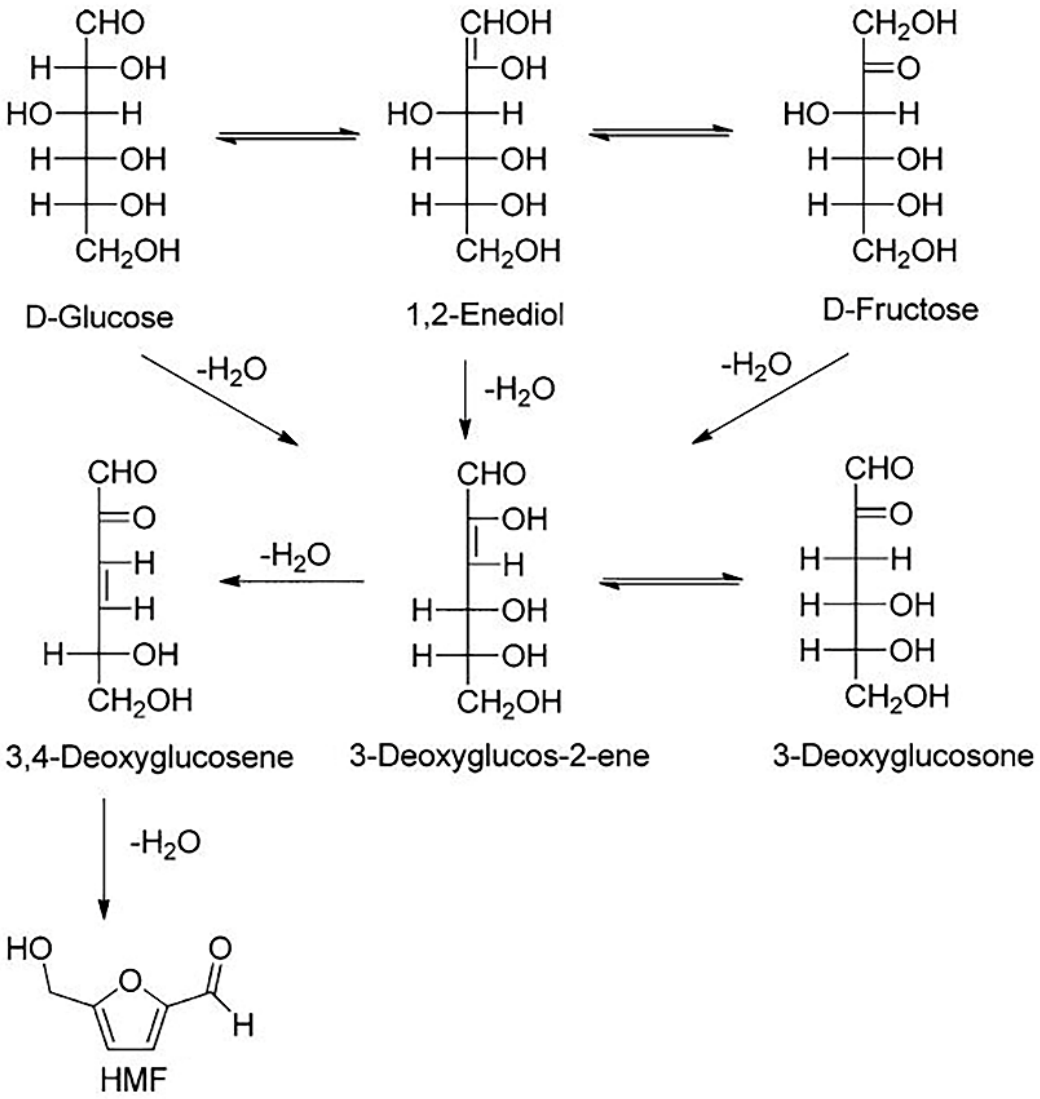

Figure 2.2 Proposed way for the dehydration of hexoses to HMF (Anet, 1964).

2.2 2,5-FURANDICARBOXYLIC ACID (FDCA)

FDCA is considered as a chemical building block (Bozell and Petersen, 2010; Bomtempo et al., 2017). It has been utilized for producing high-value chemicals (Figure 2.3) and biochemicals such as succinic acid, fungicides, thiolene films and macrocyclic ligands (Richter and Lash, 1999; Zhang et al., 2015; Larsen et al., 2018).

It can also be used as a precursor to produce polyethylene terephthalate (PET) (Davis et al., 2012; Van Nguyen et al., 2016) and surfactants (van Es et al., 2013). The use of FDCA to produce monomers like 2,5-furandicarboxylic dichloride (FDCDCl) and synthesis of nylons have been discussed by Sajid et al (2018). With the potential of wide-range of applications, FDCA has been listed as the top 12 value-added chemicals by the US Department of Energy (Werpy et al., 2004).

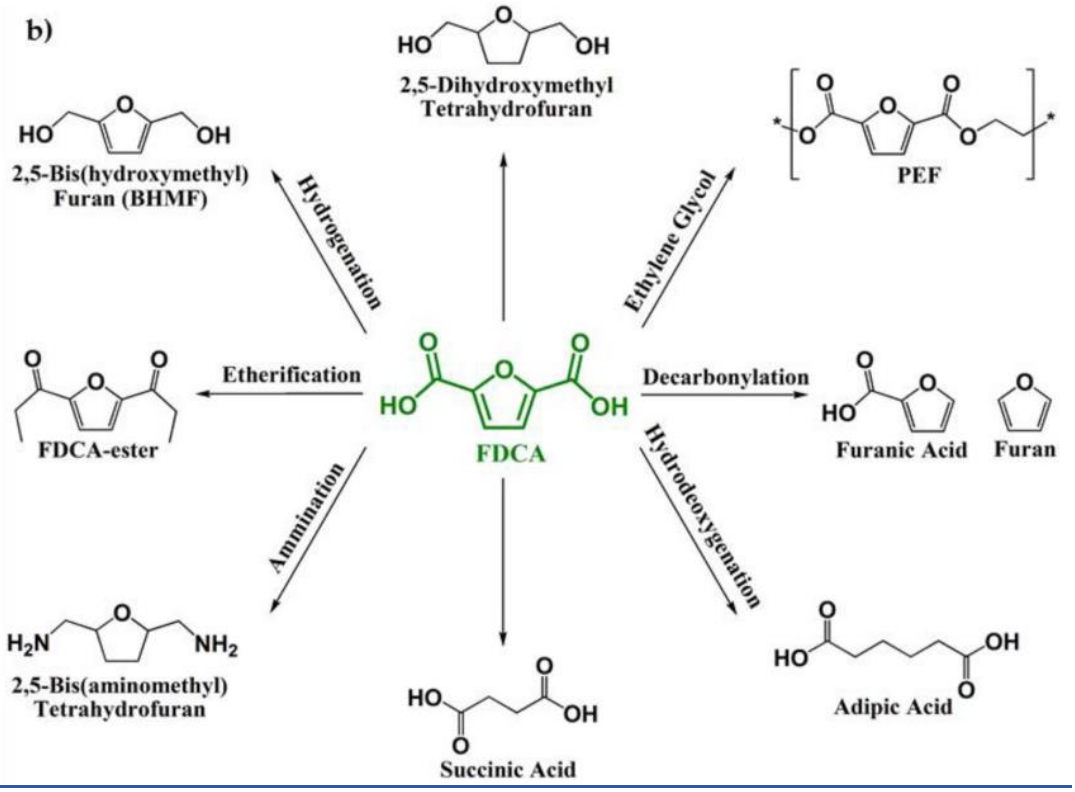

Figure 2.3 Chemicals derived from FDCA (Hameed et al., 2020).

FDCA synthesis was first reported in 1876, where mucic acid was dehydrated over strong acid catalysts (Fittig and Heinzelmann, 1876). However, the low selectivity to FDCA (<50%) and the high price of mucic acid made this process not commercially viable (Nagarkar et al., 2012). Oxidation of furfural to FDCA was discussed as a substitute method for FDCA synthesis (Gonis and Amstutz, 1962). However, the FDCA yield was low due to the complex reaction pathways that generated many by-products along the different reaction steps. Recently, selective oxidation of HMF into FDCA has been explored and considered as an environmentally benign and economical process for the production of FDCA. The oxidation can be achieved with many catalysts including homogeneous and heterogeneous catalysts,

and biocatalysts (Dijkman et al., 2014; Zhang et al., 2015; Nam et al., 2018; Xuan et al., 2018; Yan et al., 2018).

2.3 CHEMICAL OXIDATION OF HMF TO FDCA

Although electrochemical and biocatalytic oxidation HMF to FDCA has been reported recently (Dijkman et al., 2014; Cha and Chio, 2015), the synthesis of FDCA has been mainly carried out by oxidation over heterogeneous catalytic under heating. (Zhang and Deng, 2015). Compared with homogeneous catalyst, heterogeneous catalysts have drawn much more attention due to its ease of catalyst recycle and high throughput. Therefore, heterogeneous catalytic processes have a greater potential value for commercial production of FDCA from HMF.

2.4 CATALYTIC SYNTHESIS OF FDCA FROM HMF OVER SUPPORTED NOBLE METAL CATALYSTS

Recently, many studies on the oxidation of HMF over noble metal catalysts have been reported. Supported Pt, Pd, Au, and Ru catalysts were the main metal catalysts for FDCA production from HMF using oxygen as oxidant (Sankar et al., 2012). Features of the catalysts with each of the mentioned noble metals are briefed below.

4.3.1 Synthesis of FDCA from HMF over supported Pt catalysts

Pt was reported as one of the earliest heterogeneous metal catalysts for the production of FDCA from HMF. In 1993, Verdeguer and co-workers found that with the addition of Pb, Pt-Pb/C catalyst showed greater catalytic activity with the yield of 99% FDCA within 2 h whereas Pt/C catalyst only achieved 81% yield of FDCA under the same condition(Verdeguer et al., 1993). They also discovered that HMFCA was the main intermediate of HMF oxidation, indicating that the reaction path was through oxidation of carbonyl group firstly. Similarly, Bi was also used to enhance the catalytic performance of Pt/C catalyst (Rass et al., 2013). Rass and their co-workers found that the Pt-Bi/C catalyst had better stability than Pt/C catalyst, which was attributed to its high resistance to oxygen poisoning and less metal leaching with the incorporation of Bi. Beside carbon support, metal-oxide supports were also investigated. For example, Vinke et al. found more than 99% FDCA was formed over Pt/Al_2O_3 catalyst at 60 °C within 6 h (Vinke et al., 1990). Similar to Pt-Bi/C catalyst, Pt supported on CeO_2 with the addition of Bi also showed excellent catalytic performance on selectivity and stability than Pt/CeO_2 (Miao et al., 2015).

4.3.1 Synthesis of FDCA from HMF over supported Pd catalysts

Supported Pd catalysts were also widely applied in the selective oxidation of HMF (Table 2.1). David and co-workers found that Pd/C catalyst showed the comparable performance for the oxidation of HMF under a high O_2 pressure atmosphere (690 kPa), giving complete conversion of HMF with a 71% FDCA yield within 6 h (Davis et al., 2011). Later, another group developed a method to prepare uniform PVP-stabilized Pd NPs (Pd/PVP) and Pd NPs achieved the highest FDCA yield of 90% with a mean diameter of 1.8 nm under the reaction conditions at 90 °C (Siyo et al., 2014). At lower temperature (70 °C), HMFCA was the main product as the reaction rate of oxidation of FFCA to FDCA was slower than that at 90 °C, indicating the reaction temperature is a key factor for the oxidation of HMF. Based on this report, Siyo et al further studied the influence of support and various metal oxide supports such as TiO_2, Al_2O_3, ZrO_2/La_2O_3 were used (Siyo et al., 2014). Among them, ZrO_2/La_2O_3 was observed to show the highest performance for the oxidation of HMF with FDCA yield of 90%. Recently, the facet effect of Pd on the selectivity of FDCA was studied by Lei and co-workers (Lei et al., 2016). The size controllable single-crystalline Pd nanocrystal with the plane (111) and (110) was synthesized as the catalyst and they found that Pd-NOs (Pd nanooctahedrons) with the plane (111) were more active than Pd-NCs (nanocubes) with the plane (110) for the production of FDCA. Through the analysis of density functional theory (DFT), they found that the higher catalytic activity of Pd-NOs was due to the lower energy barrier in the oxidation of HMFCA to FFCA step. These reported results also indicate that it is a challenge to achieve high FDCA yield at room temperature and in 1 bar O_2. The synthetic processes at elevated temperatures and under high O_2 pressures consume more energy, which is contrary to the view of green chemistry.

Table 2. 1 Heterogeneous Pd based catalysts reported in the literature for selective synthesis of FDCA from HMF in a base solution

Entry	Catalysts	Reaction condition	FDCA Yields (%)	Ref.
1	Pd NOs	4 equiv $NaHCO_3$, 100℃, 1 bar O_2, 4 h	91.3	Lei et al., 2017
2	γ-Fe_2O_3/HAP-Pd(0)	0.5 equiv $NaHCO_3$, 100℃, 1 bar O_2, 6 h	92.9	Zhang et al., 2015
3	C/Fe_3O_4/Pd	0.5 equiv K_2CO_3, 80℃, 1 bar O_2, 4 h	91.8	Liu et al., 2015
4	Pd/ZrO_2/La_2O_3	5 equiv NaOH, 100℃, 1 bar O_2, 8 h	90.0	Siyo et al., 2014
5	Pd/C	2 equiv NaOH, 22℃, 7 bar O_2, 6 h	71.0	Davis et al., 2011
6	Pd NPs	8.5 equiv NaOH, 90℃, 1 bar O_2, 7 h	90.0	Siyo et al., 2014
7	Pd/C/Fe_3O_4	1 equiv K_2CO_3, 80℃,1 bar O_2, 6 h	86.7	Mei et al., 2015

4.3.1 Synthesis of FDCA from HMF over supported Au catalysts

In 1980s Au was reported as an effective catalyst for the oxidation of carbon monoxide, which attracts much attention (Hutchings, 1985; Harute et al., 1987). Since then, it has been applied in other oxidation reactions such as the oxidation of HMF to yield FDCA. Like the Pd and Pt based catalysts, support influences the catalytic performance of Au catalysts. Corma et al discovered that Au supported on TiO_2 and CeO_2 showed great catalytic activity than that supported on carbon or Fe_2O_3, and 99% FDCA yield was achieved over Au/TiO_2 and Au/CeO_2 catalysts after 8 h reaction at 130 ℃ under 10 bar O_2 with 4 equiv. of NaOH (Casanova et al., 2009). According to this study, the interaction between Au and CeO_2 played a role in the oxidation of alcohol group due to hydride transfer from the C-H bond to Ce^{3+} and Au^{+} spaces of Au/CeO_2. Yang and co-workers found that compared with Au/CeO_2 catalyst, the

addition of Bi to CeO_2 could greatly enhance both the O_2 adsorption and hydride transfer of CeO_2, thus enhancing the catalytic activity for the formation of FDCA. More importantly, they found that $Au/Ce_{0.9}Bi_{0.1}O_{2-\delta}$ catalyst was much more stable than Au/CeO_2 catalyst (Miao et al., 2015). Xu and co-workers also found that the supports play an important role for Au catalysts on oxidation of HMF (Cai et al., 2013). Recently, Wang and co-workers proposed a new Au/CNT catalyst for oxidation of HMF, which can be carried out in the absence of a base. However, the reaction was carried out at elevated temperature and 5 bar O_2 (Wan et al., 2014). The mechanism of oxidation of HMF to FDCA over Au catalyst was reported by Davis et al (Davis et al., 2012). To investigate the role of O_2, they carried out the reaction by using isotope labelled $^{18}O_2$ as oxidant, but they were not able to find ^{18}O from HMFCA or FDCA, indicating that O_2 was not directly involved in the reaction. Further experiments by isotope labelling technology confirmed that the O of HMFCA and FDCA comes from H_2O. Upon their finding they have confirmed that the oxidation of HMF into FDCA involves 5 steps (Figure 2.4). In the first step, HMF is converted into geminal diol intermediate via reversible hydration. Then, HMFCA is formed through dehydrogenation of geminal diol. In the third step, the oxidation of alcohol group to carbonyl group was then achieved with hydroxide ions adsorbed on the catalyst surface. The next two steps involve the oxidation of FFCA to FDCA, which were expected through the same way as the formation of HMFCA from HMF.

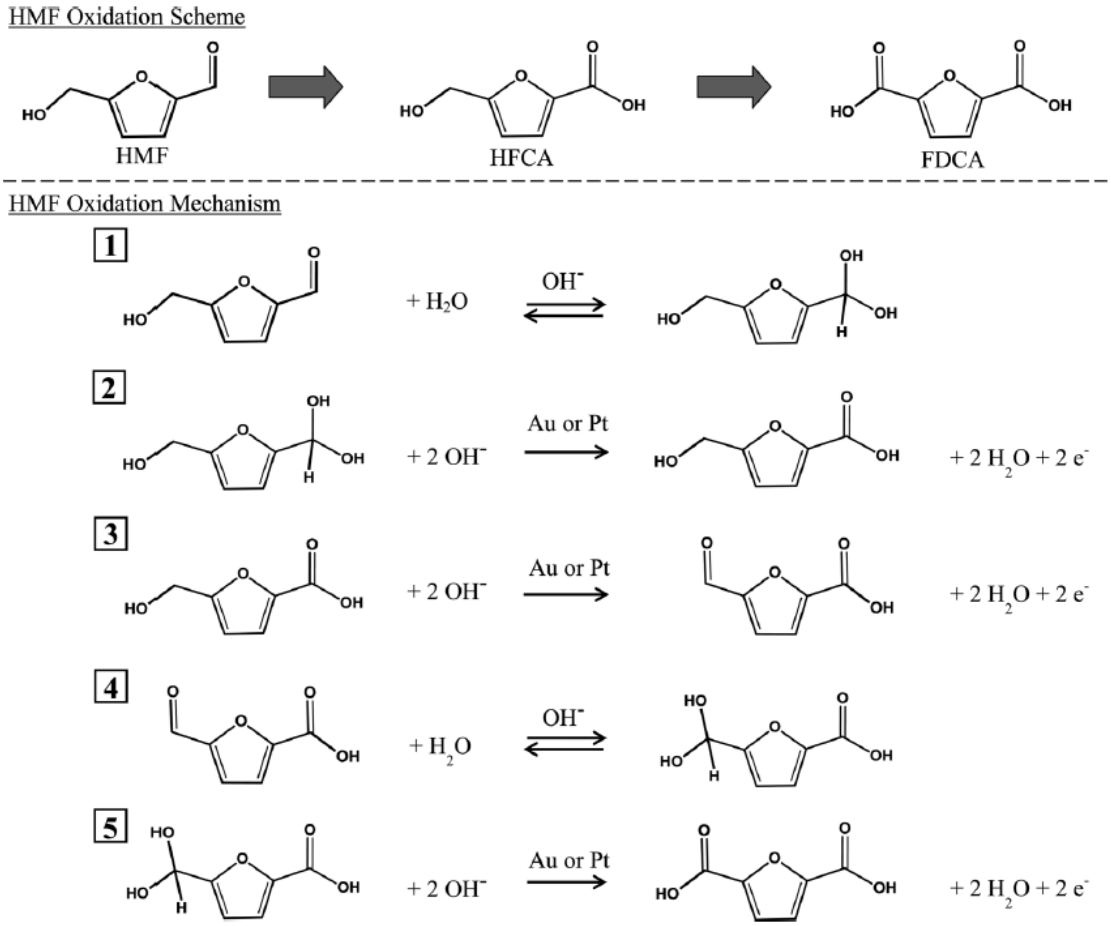

Figure 2.4 Proposed mechanism for the oxidation of HMF over Au in the presence of bases (Davis et al., 2012).

4.3.1 **Synthesis of FDCA from HMF over supported alloy catalysts**

Initially, Ru was used for the formation of DFF from HMF oxidation (Nie et al., 2013). Recently researchers have found at the lower base or base free conditions, Ru showed great catalytic performance for the oxidation of HMF to FDCA (Yi et al., 2016; Mishara et al., 2017; Pichler et al., 2018). Yi and co-workers found that the base type has a great effect on the yield of FDCA. Weak alkali $CaCO_3$ showed better selectivity to FDCA compared with strong alkali NaOH, which was attributed to the degradation of HMF at the high base condition. Many Ru-metal oxides catalysts were also applied for the oxidation of HMF to FDCA. Among these catalysts, Ru(OH)x/HT (Hydrotalcite) showed the best performance, with almost 100% FDCA yielded after 6 h at 140 ℃.

2.5 THE IMPACT OF BASE AND OXYGEN

Base and oxygen atmosphere are the most important factors for the oxidation of HMF to FDCA. It was reported that the product selectivity depends on pH. Zope et al found that the oxidation product from alcohol were primarily the intermediate aldehyde instead of acids in the absence of base. Due to the adsorbed hydroxide on the metal surface, C-H and O-H bonds activation become much effective, thus explaining the role of base (Zope et al., 2010). In addition, David et al also found that base (OH^-) can promote O-H and C-H bond activation of the alcohol side-chain of HMF and obtained aldehyde intermediate HMFCA and finally formed FDCA (Davis et al., 2012). The role of molecular oxygen in the oxidation of HMF is not obvious. Based on isotopic labelling studies from different research groups, it was believed that O_2 did not incorporate into the products. Instead, O_2 served as a scavenger of electrons deposited on the metal particles during the reaction. (Zope et al., 2010; Davis et al., 2012; Lei et al., 2016).

2.6 SUMMARY

In summary, FDCA is a very valuable platform chemical and can be applied in many fields. Although the key factors such as base and O_2 have been extensively investigated, it is still challenging to achieve the FDCA synthesis under mild conditions using metal catalysts. Due to this big research gap, it is worth developing a new catalytic system for the selective oxidation of HMF to FDCA under mild conditions.

Chapter 3: Research Design

3.1 METHODOLOGY AND RESEARCH DESIGN

The research methodology to achieve the research objectives are discussed under three main stages.

4.3.1 Synthesis of metal catalysts supported on CeO_2 nanofibre

◆ CeO_2 nanofibre was synthesized through hydrothermal reaction by controlling the temperature and concentration of base added (NaOH). The shape of CeO_2 was characterized with TEM.

◆ The catalysts were synthesised by an impregnation–reduction procedure and the size of the catalyst was controlled, adding only small amounts of an aqueous $NaBH_4$ solution dropwise. The size ranges, morphologies, and compositions of the CeO_2 support, as well as the catalyst samples, were characterised by SEM, TEM and XRD.

4.3.1 Selective aerobic oxidation of HMF to FDCA

◆ The influence of catalysts on the conversion of HMF to FDCA was investigated. AgPd alloy supported on various metal oxide catalysts for the oxidation of HMF were tested and all results measured by HPLC-MS. Based on the results

◆ The reaction conditions over AgPd catalyst, such as the reaction temperature, atmosphere, concentration of the base and alloy compositions were optimized and the results were analysed by LC-MS.

◆ The reusability of AgPd catalyst was also studied over several reaction cycles and the used catalyst was characterized by TEM, UV-visible spectra, XPS and XRD.

4.3.1 The reaction mechanism of this conversion

◆ A series of control experiments were conducted to study the mechanism of the reaction and understood the alloy effect. Calculation of adsorption energy of organic species on the catalyst was conducted using the method of density functional theory.

3.2 PARTICIPANTS

This research work was conducted by the candidate, Y. C. Jin and included setting up experiments, collection of results, data analysis, writing manuscript and thesis. Dr H. W. Liu assisted me in TEM analysis. Prof. J. F. Jia performed the calculation of adsorption energy for this work. Dr W. Martens and A/Prof. E. R. Waclawik assisted me in reviewing the manuscript. My supervisory team assisted in experiment design and editing of the manuscript before submission.

3.3 ETHICS AND LIMITATIONS

The project does not involve research into humans, animals, genetically modified organisms or biosafety materials.

Chapter 4: Experimental Section

4.1 Materials

HMF, FFCA, FDCA and sodium borohydride ($NaBH_4$) were purchased from Aladdin Chemistry Co. Ltd. HMFCA, $PdCl_2$, $AgNO_3$ were purchased from Sigma-Aldrich and used as received without further purification. The water used in all of experiment was prepared by passage through an ultrapurification system.

4.2 Preparation of catalysts

CeO_2 fibre. the CeO_2 support was prepared via reported method[1]. NaOH pellets and $Ce(NO_3)_3{\cdot}6H_2O$ (both are AR grade and from Aldrich) were used in the synthesis. In a typical way, 1.302 g of $Ce(NO_3)_3{\cdot}6H_2O$ was dissolved in 7.5 ml deionized water, and 14.4 g NaOH was dissolved in 52.5 ml of respectively. Then the mixture was transferred in a stainless autoclave with a poly (tetrafluoroethylene) (PTFE) container and was maintained at 100 ℃ for 24 h. Upon leaving the solution cool to room temperature, the solid was recovered from the autoclaved mixture, rinsed with water and ethanol several times. Finally, the results were dried at 50℃ for 1 day.

Ag-Pd/CeO_2 Catalysts. Catalysts of alloy NPs with various Ag:Pd ratios on the CeO_2 support were prepared via an impregnation–reduction procedure as described in our previous paper.[2] For example, 1.5 wt% Ag-1.5wt %Pd/CeO_2 was prepared by the following procedure: 2.0 g CeO_2 powder was dispersed into 15.2 mL of 0.01 M $AgNO_3$ aqueous solution and 28.3 mL of 0.01 M $PdCl_2$ aqueous solution was added while magnetically stirring. To this suspension, 15 mL of 0.6 M $NaBH_4$ solution was added dropwise in 60 min. The mixture was aged for 24 h and then the solid was separated, washed with water (three times) and ethanol (once), and dried at 60 °C. The dried solid was used directly as the catalyst. Catalysts with other Ag:Pd ratios were prepared in a similar method but using different quantities of $AgNO_3$ aqueous solution and $PdCl_2$ aqueous solution. The obtained catalysts were labelled as Ag_xPd_{3-x} (e.g., $Ag_{1.5}Pd_{1.5}/CeO_2$ contains 1.5 wt% Ag and 1.5 wt% Pd).

4.3 Catalyst characterization

The sizes, morphologies, and compositions of the catalyst samples were characterised by Transmission Electron Microscopy (TEM) using a JEOL 2100 transmission electron microscope equipped with a Gatan Orius SC1000 CCD camera and an Oxford X-Max EDS instrument. The metal contents of the prepared catalysts were determined by Energy Dispersion X−ray Spectrum (EDS) technology on JEOL 7001F with oxford EDS detector using Aztec software. The X-ray Diffraction (XRD) was recorded on a Rigaku smartlab X-ray diffractometer with Cu Kα radiation of 1.5418 Å. DR-UV-vis spectra of the samples were obtained using a Varian Cary 5000 spectrometer.

4.4 Catalytic reaction

A 20 mL Pyrex glass tube was used as the reaction container, and after the reactants and catalyst had been added, the tube was bubbled with O_2 for 5min and sealed with a rubber septum cap. All the reactions were conducted using an oil bath placed above a magnetic stirrer to control the reaction temperature and the temperature of the oil bath is 20 °C. The reaction was under stirring, and the start time was recorded. 2 mL aliquots were collected, centrifuged, and then filtered through a Millipore filter (pore size 0.45 μm) to remove the catalyst particulates. The filtrates were analysed by high performance Liquid Chromatography (Dionex Ultimate HPLC) and LTQ Orbitrap Elite Mass Spectrometer.

The adsorption experiment was performed by addition of 50 mg $Ag_{1.5}Pd_{1.5}/CeO_2$ catalyst into 10 mL of aqueous solution containing 7.5 mg fulvic acid. The suspension was stirred for 30min at room temperature. The amount of fulvic acid adsorbed on the catalyst was measured by UV-visible spectra.

4.5 ANALYSIS

The results of oxidation of HMF were analysed by high performance liquid chromatography (Dionex Ultimate HPLC) and LTQ Orbitrap Elite Mass Spectrometer (LC-MS) at 30 °C using a C18 column and a UV detector to measure the concentration change of reactants and products. The mobile phase consists of 0.4% formic acid in water, and pure acetonitrile (60:40, v/v) at flow rate of 0.4 mL/min was used. The absorption wavelength of the UV detector was set to 260 and 280 nm.

The commercial standard compounds (HMF, HMFCA, DFF, FFCA, FDCA) were purchased as standards to identify the products of HMF oxidation by comparing their retention time. The conversion of HMF and the product yields have been calculated by the external standard method using HPLC. The HMF conversion and HMFCA yield were calculated as follows:

Conversion % = HMF mole after the reaction/HMF mole before the reaction × 100%.

Yield % = Product mole after the reaction/HMF mole before the reaction × 100%.

The speed of reaction was calculated according to the reported method (Ait Rass et al., 2015). Equations 1−4 give the rate equations for each species consumed and formed, where C_{HMF}, C_{HMFCA}, C_{FFCA}, and C_{FDCA} are the concentrations of the participating reactants and products, and k_1−k_3 are the catalytic constants of each reaction step (Scheme 4.1). To estimate the kinetic parameters of different oxidation steps, the typefitting of MATLAB was used.

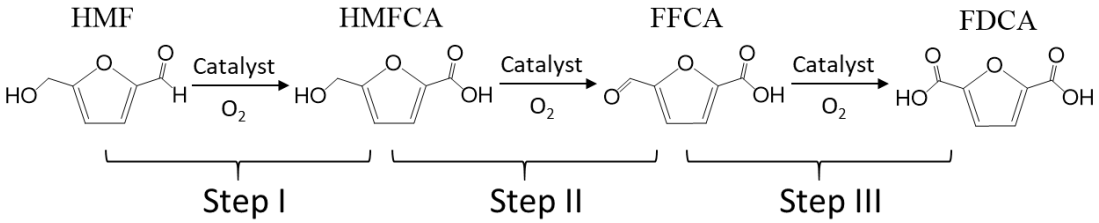

Scheme 4.1. Scheme of selective oxidation of HMF. The oxidation involves three steps (Delidovich et al., 2016).

$$\frac{dC_{HMF}}{dt} = -k_1 C_{HMF} \quad (1)$$

$$\frac{dC_{HMFCA}}{dt} = k_1 C_{HMF} - k_2 C_{HMFCA} \quad (2)$$

$$\frac{dC_{FFCA}}{dt} = k_2 C_{HMFCA} - k_3 C_{FFCA} \quad (3)$$

$$\frac{dC_{FDCA}}{dt} = k_3 C_{FFCA} \quad (4)$$

Chapter 5: Results and Discussion

Chapter 5 is provided in 4 parts to match the objective of this study:

- Screening - Research Objective 1
- Reaction parameters - Research Objective 2
- Mechanism study - Research Objective 3
- Reusability – Research Objective 4

5.1 SCREENING - RESEARCH OBJECTIVE 1

The screening tests for the oxidation of HMF was shown in Table 5.1, an excellent yield (93%) of FDCA was achieved over $Ag_{1.5}Pd_{1.5}/CeO_2$ catalyst with 4 h. Only a small amount of intermediates were detecte. The control experiment showed that the yield decreased to 45.7% and 0% when the reaction was conducted over $Pd_{3.0}/CeO_2$ and $Ag_{3.0}/CeO_2$ catalysts while other reaction conditions were identical. This confirms that Ag-Pd alloy NPs significant enhanced reaction performance. To investigate the parameters of the reaction, catalyst composition (Figure. 5.1), catalyst support materials (Figure. 5.2), base concentration (Figure. 5.3) and atmosphere (Table 5.2) were studied.

Table 5.1 Catalyst screening for the selective oxidation of HMF [a]

Entry	Catalyst	HMF conv. (%)	HMFCA yield(%)	FFCA yield (%)	FDCA yield (%)	TON[b](Pd)
1	$Ag_{1.5}Pd_{1.5}/CeO_2$	100	3.0	0	93.0	49.2
2	$Pd_{3.0}/CeO_2$	100	38.1	16.1	45.7	12.2
3	$Pd_{1.5}/CeO_2$	100	35.0	10.0	20.0	10.6
4	$Ag_{3.0}/CeO_2$	100	70.0	0	0	0
5	$Ag_{1.5}/CeO_2$	100	75.0	0	0	0
6	CeO_2	100	2.5	0	0	0
7	No catalyst	100	0	0	0	0

[a] Reaction conditions: HMF (0.15 mmol), 20mg catalysts, NaOH (0.4 mmol), 3 mL of the solvent H_2O, 20 °C, 4 h under an 1 bar oxygen atmosphere. [b] TON was calculated based on the amount of Pd.

5.2 REACTION PARAMETERS - RESEARCH OBJECTIVE 2

As shown in Fig 5.1, a series of catalysts with different contents of AgPd alloy NPs supported on CeO_2 were prepared. These catalysts were labeled as Ag_xPd_{3-x} (e.g., $Ag_{1.5}Pd_{1.5}/CeO_2$ contains 1.5 wt% Ag and 1.5 wt% Pd). 3.0 wt% AgPd alloy ($Ag_{1.5}Pd_{1.5}/CeO_2$) exhibited the best catalytic performance for the oxidation of HMF. As the alloy content of the catalyst increased from 1% to 3 wt%, the FDCA yield increased from 6.7% to 67.5% after 3 h reaction. When the content increased from 3 wt% to 5 wt%, the FDCA yield is still lower than that achieved on $Ag_{1.5}Pd_{1.5}/CeO_2$ catalyst.

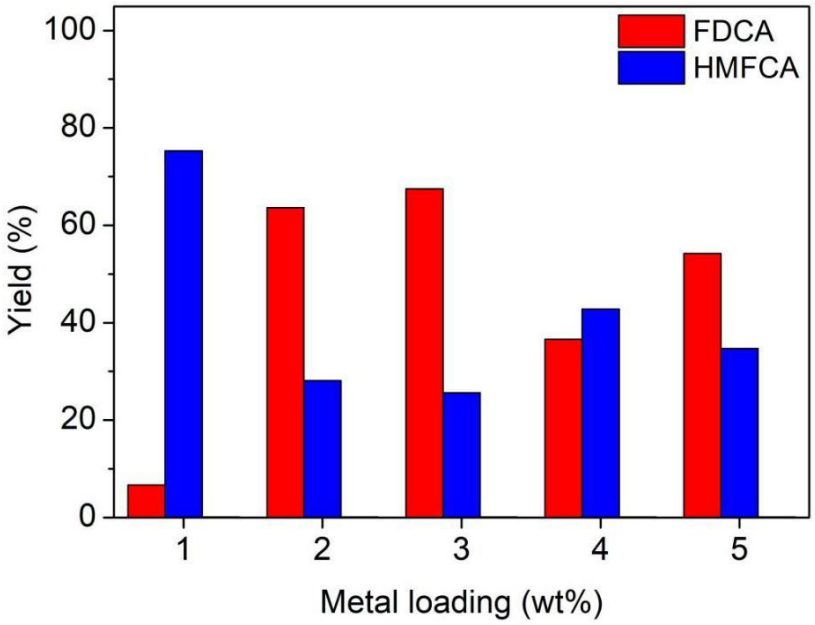

Figure 5.1 Product selectivity for the oxidation of HMF on AgPd/CeO_2 with various total metal loadings (Ag:Pd ratio =1). Reaction conditions: HMF (0.15 mmol), 20 mg catalysts, NaOH (0.4 mmol), 3 mL of the solvent H_2O, 20 °C, 3 h under an 1 bar oxygen atmosphere.

Ag-Pd alloy NPs was further supported on different materials (Figure. 5.2). CeO_2 showed the highest catalytic activity with the highest yield of FDCA (93%). This is due to CeO_2 fibril support is not only good for the diffusion of reactant and product but also strongly binds noble metal NPs and adsorbs O_2 (Huang et al., 2005; Montini et al., 2016; Lei et al., 2020). These properties benefit the catalytic performance for the selective oxidation using O_2 as oxidant and stability of the catalysts. Figure 5.3 shows that the FDCA yield increased with the amount of NaOH increased. With no addition of base, the reaction rate of oxidation of HMFCA was extremely lower, which was consistent with the previous literature (Davis et al., 2012).

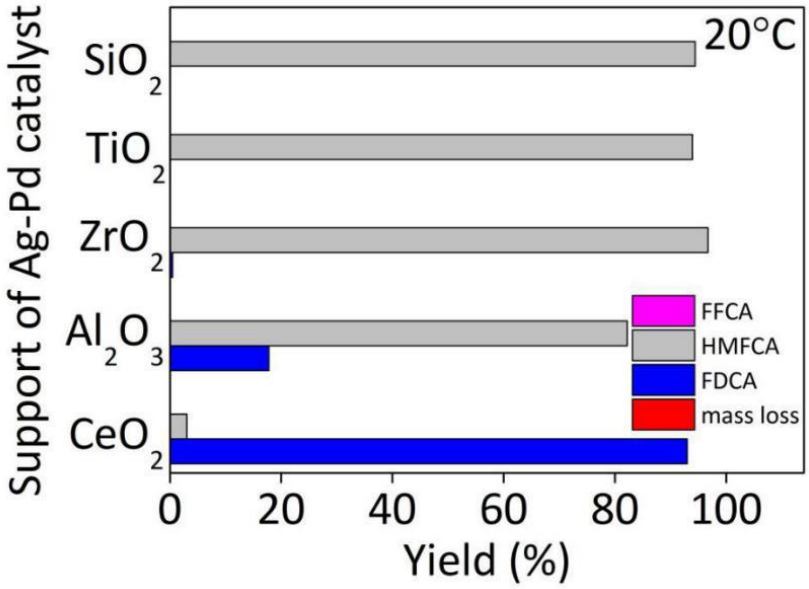

Figure 5.2 Catalytic performance of $Ag_{1.5}Pd_{1.5}$ alloy nanoparticles loaded on various supports for aerobic oxidation of HMF. Reaction conditions: HMF (0.15 mmol), 20 mg catalysts, NaOH (0.4 mmol), 3 mL of the solvent H_2O, 20 °C, 4 h under an 1bar oxygen atmosphere.

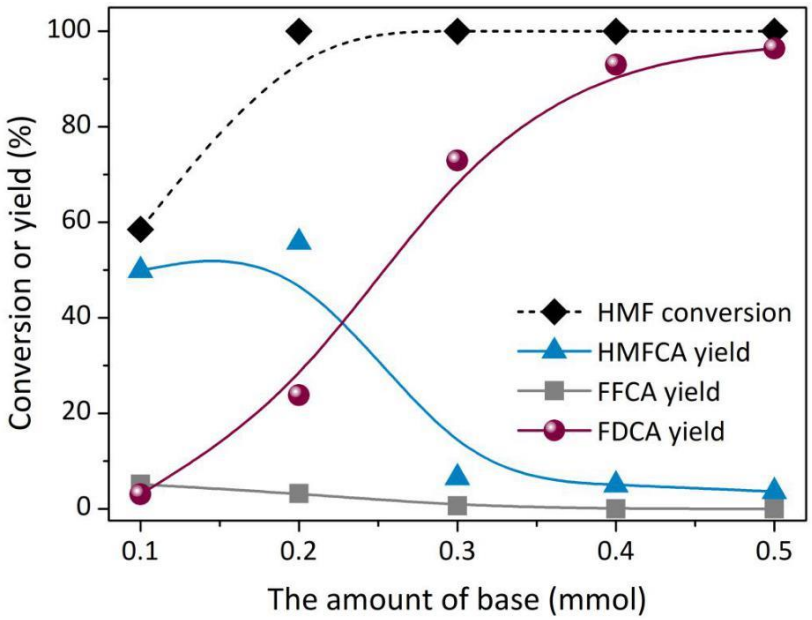

Figure 5.3 Effect of base concentration on the conversion from HMF to FDCA. Reaction conditions: HMF (0.15 mmol), 20 mg catalyst, varied amount of NaOH, 3 mL of the solvent H_2O, 20 °C, 4 h under a 1 bar oxygen atmosphere.

The results listed in Table 5.2 show the effect of the atmosphere on the yield of FDCA. In an oxygen atmosphere, an FDCA yield of 93% with the HMF conversion of 100% was achieved. However, in air or argon, a much lower FDCA yield (41.8% or 8.5%) was obtained. The results indicate that oxygen is the oxidant for the conversion from HMFCA to FDCA, which is consistent with the results reported in the literature (Hayashi et al., 2019; Xu et al., 2017). According to the study of Davis and Gorbanev, an oxygen free atmosphere, HMF was simultaneously oxidised to HMFCA and reduced to BHMF in basic reaction medium via the Cannizzaro reaction, and no FDCA was obtained over Au and Pt catalyst, which also indicates that FDCA cannot be obtained under oxygen-free condition (Davis et al., 2012; Gorbanev et al., 2009).

Table 5.2 Effect of atmosphere on the selectivity of FDCA

Entry	Atmosphere	HMF conversion (%)	HMFCA yield (%)	FFCA yield (%)	FDCA yield (%)
1	1 bar O_2	100	3.0	0.0	93.0
2	1 bar Air	100	54.0	0.0	41.8
3	1 bar Ar	100	81.2	0.0	8.5

Reaction conditions: HMF (0.15 mmol), 20 mg catalysts, NaOH (0.4 mmol), 3 mL of the solvent H_2O, 20 °C, 4 h under varies atmosphere (1 bar).

Based on these results, we found that such a relay of catalysis over the catalyst containing 1.5 wt% Ag and 1.5 wt% Pd on CeO_2 support ($Ag_{1.5}Pd_{1.5}/CeO_2$) exhibits an optimal FDCA yield (93%) in basic aqueous solution and 1 bar O_2 atmosphere at 20 °C (Figure. 5.4A), that is superior to Pd-based catalysts reported in the literature for driving this reaction in terms of FDCA yield and reaction conditions as the comparison shows in Table 2.1. Complete conversion of HMF to FDCA over $Ag_{1.5}Pd_{1.5}/CeO_2$ catalyst at 20 °C can be achieved within 10 h (Figure. 5.5a). The slow conversion after 4 h reaction was attributed to the strong adsorption of FDCA on the alloy catalyst (see Table 5.3), resulting in slow FDCA desorption from the catalyst. The FDCA yield achieved on $Pd_{3.0}/CeO_2$ catalyst was 35%. When the reaction time is prolonged to 10 h, the yield is still lower than that achieved on $Ag_{1.5}Pd_{1.5}/CeO_2$ within 4 h (Figure. 5.5b). The Pd-based catalysts required elevated temperature and high oxygen pressure to produce FDCA from HMF. To the best of our knowledge, there has been no report yet on AgPd alloy catalyst used for the oxidation of HMF.

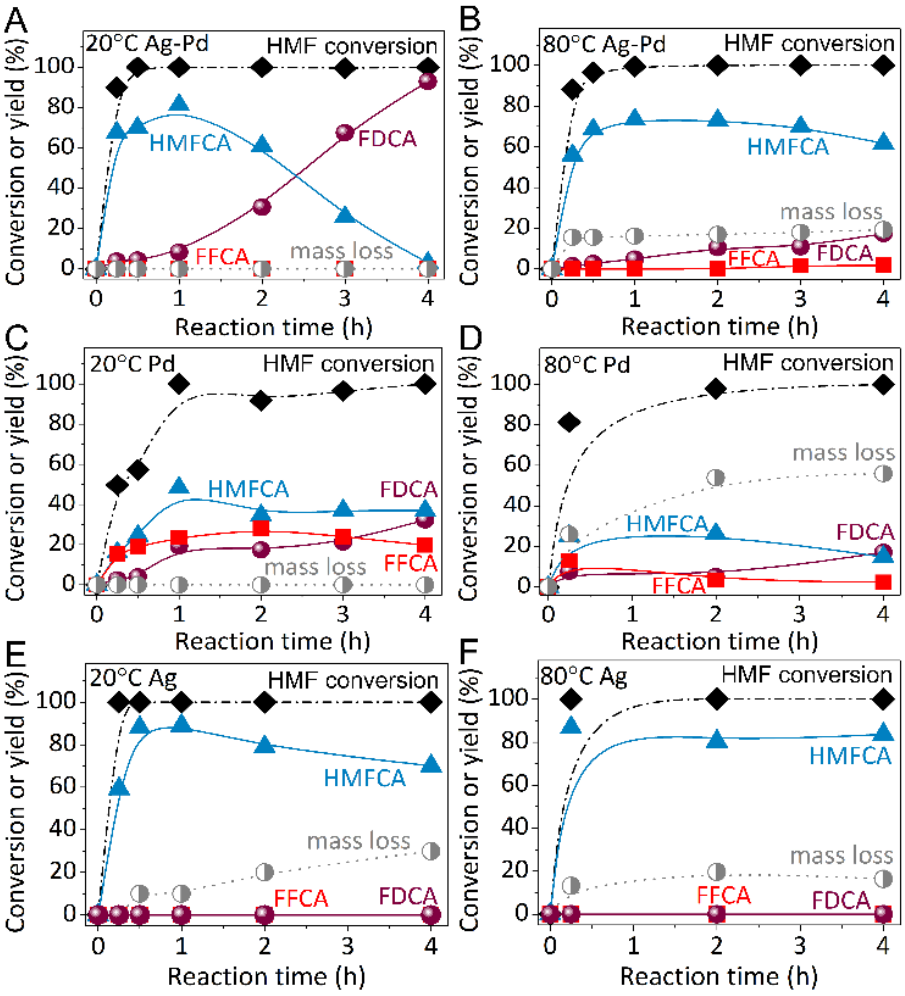

Figure 5.4 Time–course product selectivity of HMF oxidation reaction over $Ag_{1.5}Pd_{1.5}/CeO_2$ at 20 °C (A) and 80 °C (B), over $Pd_{3.0}/CeO_2$ at 20 °C (C) and 80 °C (D), and over $Ag_{3.0}/CeO_2$ at 20 °C (E) and 80 °C (F). Conditions: 1 bar O_2 atmosphere, 3 mL of deionised water mixed with 0.15 mmol of HMF, 20 mg catalyst and 0.4 mmol NaOH and the reaction time was 4 h. All HMF conversion reached 100% after 2h (black dash dot line).**Error! Use the Home tab to apply 标题 1 to the text that you want to appear here.**

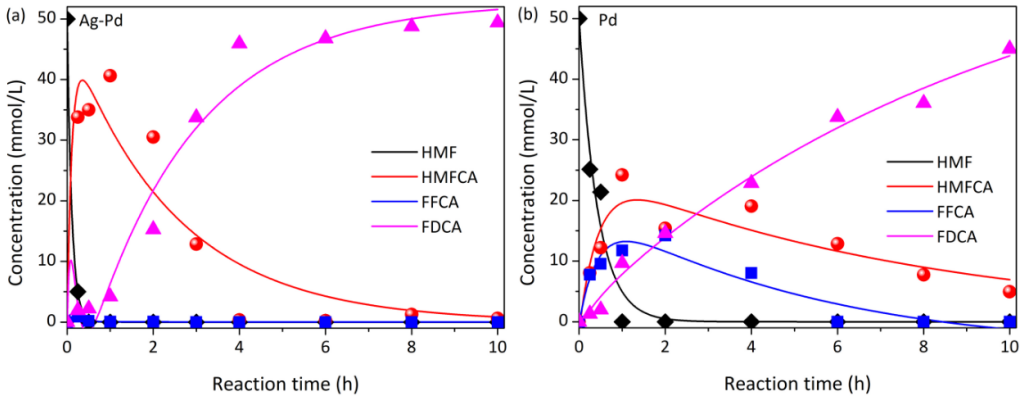

Figure 5.5 Experimental data (points) and model estimates (continuous lines) for HMF oxidation over (a) $Ag_{1.5}Pd_{1.5}/CeO_2$ and (b) $Pd_{3.0}/CeO_2$

Table 5.3 Adsorption amounts during the co-adsorption of HMF and possible intermediate (HMFCA and FFCA) and product (FDCA) from aqueous solutions onto different catalysts at room temperature

Catalyst	Adsorption amount[a] (µmol per gram of catalyst)			
	HMF	HMFCA	FFCA	FDCA
$Ag_{1.5}Pd_{1.5}/CeO_2$	9.2	26.1	29.0	90.3
$Pd_{3.0}/CeO_2$	9.7	29.1	29.1	92.3
$Ag_{3.0}/CeO_2$	9.4	69.1	73.1	99
CeO_2	4.2	59.3	70.6	98.4

[a] The adsorption was performed by addition of 100 mg catalyst into 10 mL of aqueous solution containing 10 µmol HMF, HMFCA, FFCA and FDCA. The suspension was stirred for 2 h at room temperature, followed by resting for another 2 h.

5.3 MECHANISM STUDY - RESEARCH OBJECTIVE 3

Interestingly, the product selectivity of the cascade oxidation over alloy catalyst shifts towards the intermediate product HMFCA when the reaction temperature is increased to 80 °C (Figure. 5.4B). The FDCA yield at 80 °C is less than 20%, and the upper stream product HMFCA is predominantly formed instead (~80%). This is an atypical phenomenon. Usually, in the oxidation of a compound with O_2, heating facilitates the formation of the most oxidised final product. However, in the present study, high selectivity to final product FDCA for the selective oxidation is achieved at

low temperature and the selectivity to an intermediate HMFCA is achieved at high temperatures.

The time course of the reaction at 20 °C (Figure. 5.4A) confirms that the first step of the HMF oxidation is the same as that illustrated in Scheme 1, yielding HMFCA. When the $Ag_{3.0}/CeO_2$ catalyst was used, trace ring-opening products were detected, but no FFCA and FDCA yielded and the main product was HMFCA (Figures. 5.4E, 5.4F and 5.6C). The $Ag_{3.0}/CeO_2$ catalyst was unable to catalyse the oxidation of the alcohol group of HMFCA, which is consistent with results reported in the literature (Zhang et al., 2014; An et al., 2019). An FFCA yield of 16.1% was observed over the $Pd_{3.0}/CeO_2$ catalyst (see Figure. 5.4C). FFCA is the product of the second step before forming FDCA (Scheme 1). Negligible FFCA intermediate was observed over $Ag_{1.5}Pd_{1.5}/CeO_2$, as it was oxidised to FDCA rapidly. FFCA transformed to FDCA via oxidation of its carbonyl to a carboxyl, which can be catalysed by both Ag and Pd surface sites (Figure. 5.7). The surface of $Ag_{1.5}Pd_{1.5}$ alloy NPs appears the most efficient for this oxidation in the presence of HMF, HMFCA and FDCA.

To gain insight into the reaction process on the alloy catalyst, we estimated the rate constants for HMF, HMFCA and FFCA oxidation over the three catalysts from the data of Figure. 5.4, respectively. Calculation details are provided in Section 3.5. The rate constant of oxidising HMFCA over $Ag_{1.5}Pd_{1.5}/CeO_2$, $k_{HMFCA,\ AgPd}$, is 0.40 h^{-1}, lower than the constants for oxidising HMF ($k_{HMF,\ AgPd}$ = 9.29 h^{-1}) and oxidising FFCA ($k_{FFCA,\ AgPd}$ = 8.84 h^{-1}). The step of oxidising HMFCA is the rate-determining step of the cascade reaction, yielding FDCA from HMF over the alloy catalyst. In comparison, the rate constants over $Pd_{3.0}/CeO_2$ catalyst are much lower ($k_{HMFCA,\ Pd}$, = 0.13 h^{-1} and $k_{FFCA,\ Pd}$ = 0.08 h^{-1}), and the rate-determining step over $Pd_{3.0}/CeO_2$ catalyst is oxidation of FFCA. Alloying Ag with Pd significantly promotes the oxidation of the carbonyl groups in the intermediate FFCA at 20 °C, changing the rate-determining step to oxidation of HMFCA. This step takes place on Pd surface sites. The dependence of HMFCA oxidation on the reaction temperature should provide an explanation why the product selectivity is switched by the reaction temperature and the configurations of Pd atoms at the alloy NP surface provide the reason why $Ag_{1.5}Pd_{1.5}/CeO_2$ catalyst is superior to $Pd_{3.0}/CeO_2$ catalyst for catalysing the selective oxidation of HMF to yield FDCA.

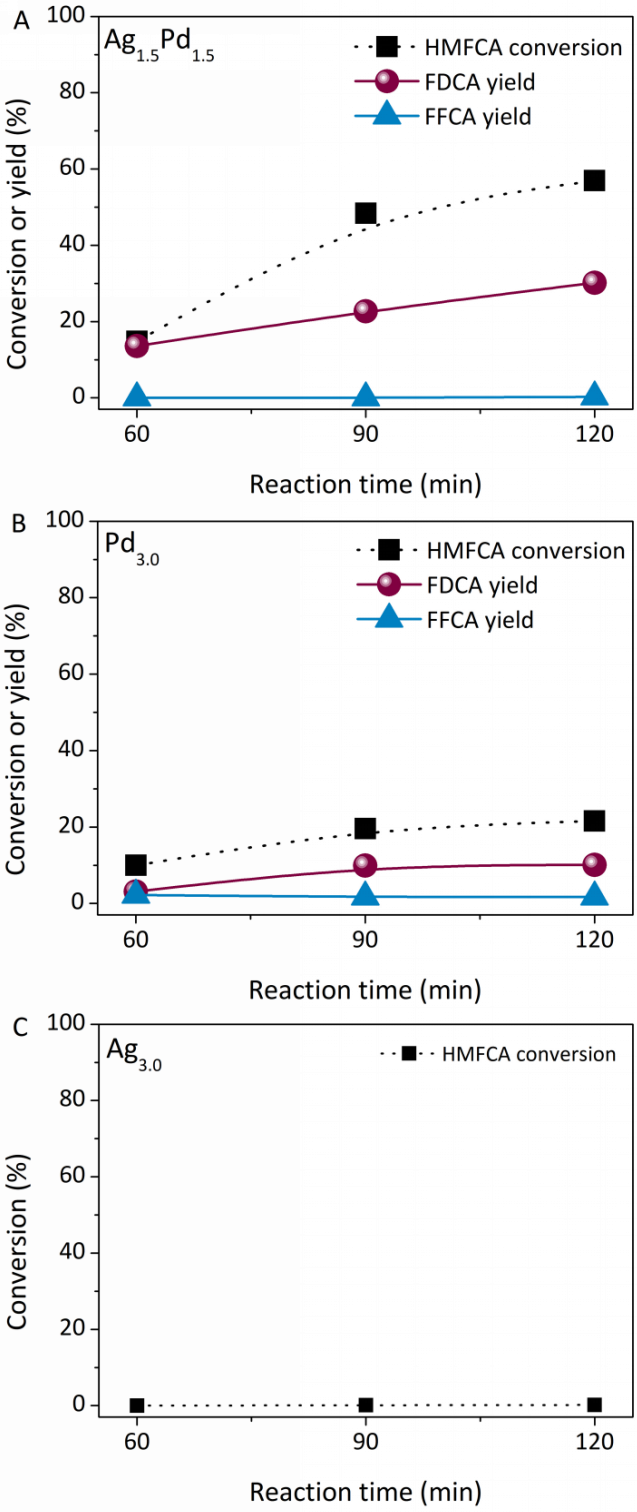

Figure 5.6 (A, B and C) Time−conversion plots for the oxidation of HMFCA using (A) $Ag_{1.5}Pd_{1.5}/CeO_2$, (B) $Ag_{3.0}/CeO_2$ and (C) $Pd_{3.0}/CeO_2$ as the catalyst. The reactions were conducted in a 1 bar oxygen atmosphere at 20 °C using 2 mL of deionized water mixed with 0.04 mmol of NaOH, 0.015 mmol of HMFCA, and 20 mg of catalyst.

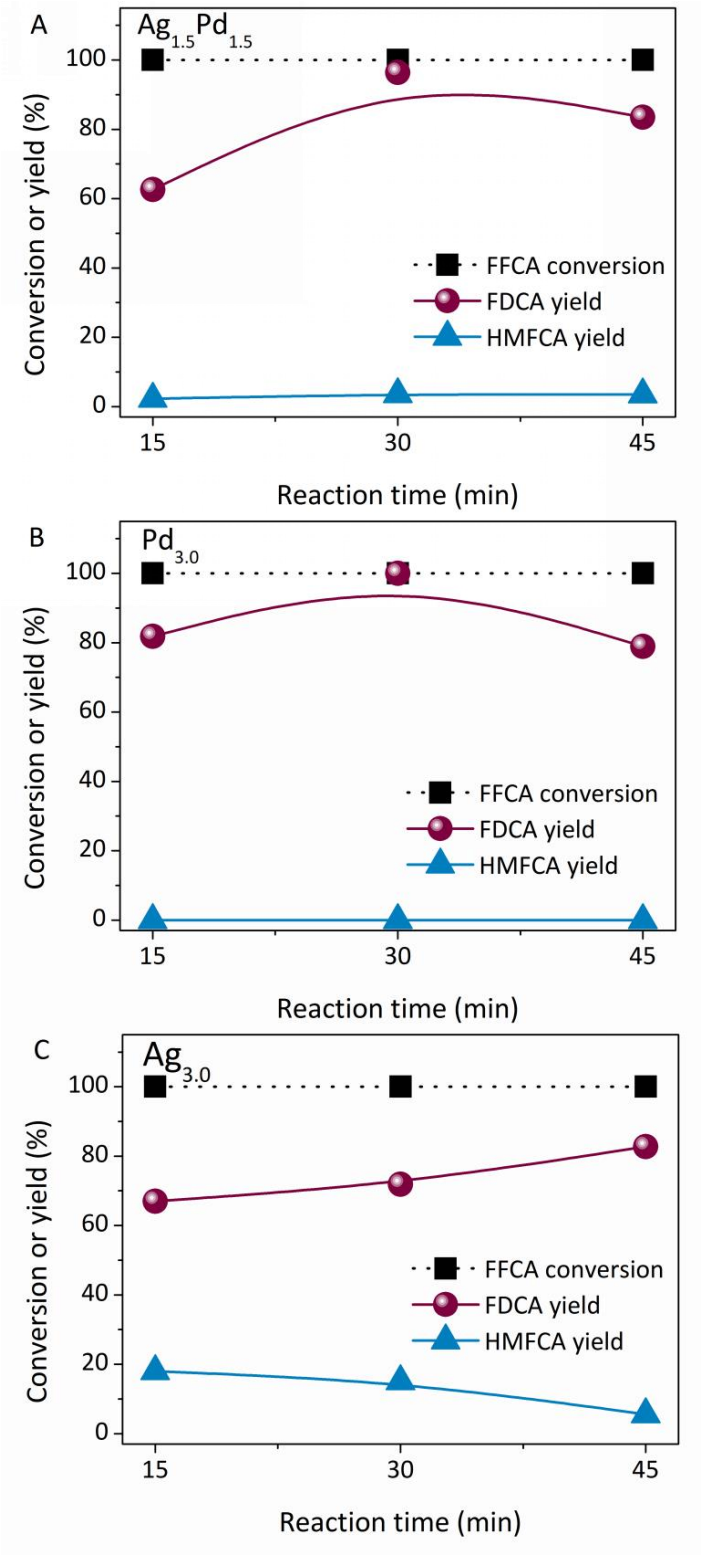

Figure 5.7 (A, B and C) Time−conversion plots for the oxidation of FFCA using (A) $Ag_{1.5}Pd_{1.5}/CeO_2$, (B) $Ag_{3.0}/CeO_2$ and (C) $Pd_{3.0}/CeO_2$ as the catalyst. The reactions were conducted in a 1 bar oxygen atmosphere at room temperature (20 °C) using 3 mL of deionized water mixed with 0.8 mmol of NaOH, 0.015 mmol of FFCA, and 20 mg of catalyst.

Figure. 5.8A shows that the HMFCA yield increases as the reaction temperature is raised. This can be attributed to HMFCA oxidation over the AgPd alloy catalyst decreasing at higher temperatures, Figure. 5.4A and 5.4B show that the HMFCA oxidation over the AgPd alloy at 80 °C is much slower than that at 20 °C. Such a trend is distinct from the common observation that oxidation reactions with O_2 as oxidant are usually accelerated with heating. The unusual trend is responsible for the product selectivity switch with the reaction temperature. The conversion of HMFCA also decreases at a higher temperature (80 °C) on Pd NPs (Figure. 5.4D), compared with that at 20 °C (Figure. 5.4C). It appears that the Pd surface sites of the catalysts exhibit lower catalytic activity at 80 °C.

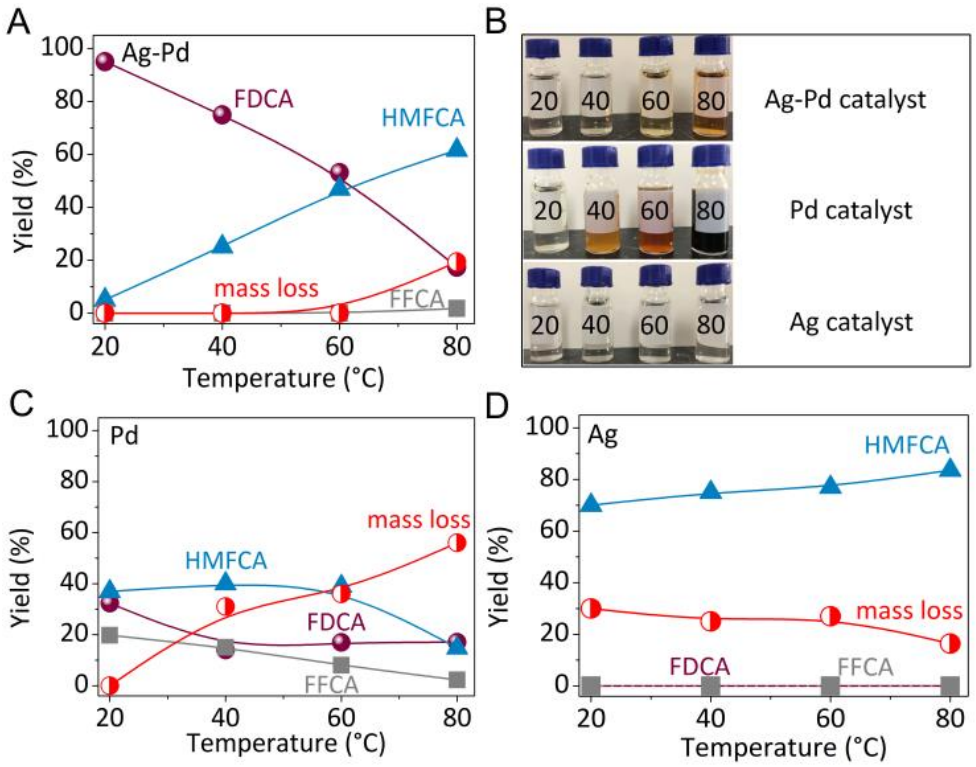

Figure 5.8 Impact of reaction temperature on the product selectivity of HMF oxidation reaction catalysed by AgPd alloy catalyst (A), Pd NP catalyst (C) and Ag NP catalyst (D), respectively. (B) The image of the product solution obtained at different treatment. The reaction conditions were the same as those given in Figure. 1, except the temperature changes.

From Figures 5.4 and 5.8, we find that the performance deterioration of $Pd_{3.0}/CeO_2$ and $Ag_{1.5}Pd_{1.5}/CeO_2$ catalysts at 80 °C is accompanied by mass loss. Carbon balance of several reactions is less than 100% (the carbon content in the product is less than the content in reactant HMF), the difference in carbon content is

indicated by mass loss (in percentage). As mass loss increases (Figures. 5.8A and 5.8C), the colour of the supernatants collected after the reactions becomes darker (Figure. 5.8B). The results of liquid chromatography-mass spectrometry confirm that the coloured supernatants contain large molecules (Figure. 5.9), the species with the highest abundance have a molecular mass of 286. They are consistent with the literature reports (Mika et al., 2018; Nakagawa et al., 2013; Patil and Lind, 2011; Tsilomelekis et al., 2016). The mass losses are due to side-reaction during the selective oxidation of HMF, which yield large molecule by-products. The mass losses in the reaction catalysed by $Ag_{3.0}/CeO_2$ are observed even at 20 °C, but the supernatant is clear. The losses are due to the strong adsorption of the HMFCA on the catalyst (Table 5.3). The by-products are formed on the Pd surface sites of the catalysts. This finding was also observed by Zhang et al. (Zhang et al., 2015)

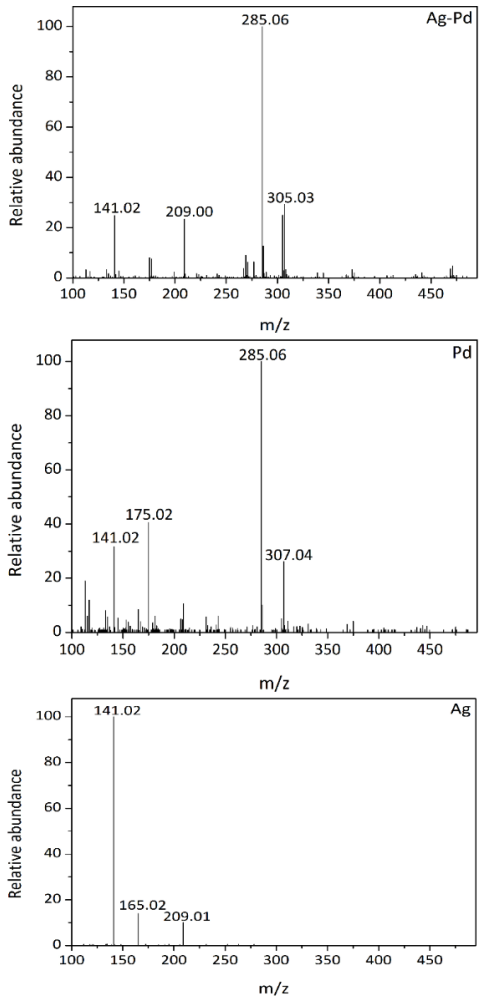

Figure 5.9 Liquid Chromatograph-Mass-Spectrometry (LC-MS) spectra of the supernatants collected in negative reflectron mode after the reaction catalyzed by $Ag_{1.5}Pd_{1.5}/CeO_2$ and $Pd_{3.0}/CeO_2$. The reactions were conducted at 80 °C.

Figures 5.4 and 5.8 also show that the more mass loss, the worse performance of $Pd_{3.0}/CeO_2$ and $Ag_{1.5}Pd_{1.5}/CeO_2$ catalysts are for oxidation of HMFCA (and thus FDCA yield). The formation of the large molecule by-products on Pd surface sites impedes the HMFCA oxidation. This is supported by observation that after adsorbing fulvic acid, $Ag_{1.5}Pd_{1.5}/CeO_2$ catalyst lost most catalytic activity for oxidation of HMFCA (Table 5.4 and Figure. 5.10). When the reaction temperature is raised, the formation of unwanted product over $Ag_{1.5}Pd_{1.5}/CeO_2$ and $Pd_{3.0}/CeO_2$ catalysts increases, as reflected by the mass loss (Figures. 5.8A-5.8C). At 20 °C the formation of by-products during the reaction catalysed with $Ag_{1.5}Pd_{1.5}/CeO_2$ is negligible. Besides, the mass losses on $Pd_{3.0}/CeO_2$ catalyst are more serious than that on $Ag_{1.5}Pd_{1.5}/CeO_2$ at all temperatures (Figure. 5.8), indicating that alloying Ag with Pd effectively alleviates the formation of the unwanted by-products. Thus, the efficient oxidation with $Ag_{1.5}Pd_{1.5}/CeO_2$ catalyst at 20 °C effectively avoids by-product formation and is an efficient and green process.

Table 5.4 The influence of fulvic acid adsorbed on $Ag_{1.5}Pd_{1.5}$ catalyst [a] on the product selectivity of HMF oxidation

Entry	Catalyst	HMF conv. (%)	HMFCA yield (%)	FFCA yield (%)	FDCA yield (%)	Mass loss (%)
1	$Ag_{1.5}Pd_{1.5}/CeO_2$ after adsorption of fulvic acid	100	87.9	0	6.8	5.3

Conditions: HMF (0.15 mmol), 20 mg $Ag_{1.5}Pd_{1.5}$ catalysts (adsorbed fulvic acid), NaOH (0.4 mmol), 3 mL of the solvent H_2O, 20 °C, 4 h under a 1 bar oxygen atmosphere. [a] Adsorption details: The adsorption was performed by addition of 50 mg $Ag_{1.5}Pd_{1.5}/CeO_2$ catalyst into 10 mL of aqueous solution containing 7.5 mg fulvic acid. The suspension was stirred for 30 min at room temperature. The amount of fulvic acid adsorbed on the catalyst was measured by UV-visible spectra. By calculation, 5 mg fulvic acid was adsorbed on 50 mg $Ag_{1.5}Pd_{1.5}/CeO_2$. After adsorption, the catalyst was then dried in a vacuum oven at 60 °C.

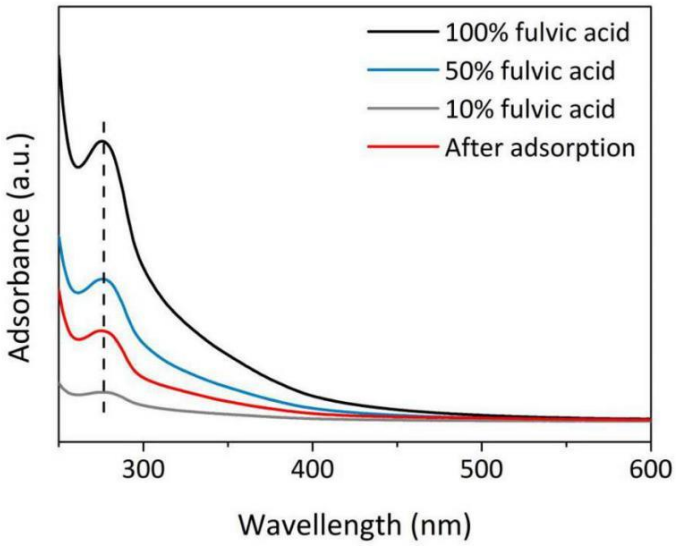

Figure 5.10 UV-vis spectra of the standard fulvic acid solution and the result solution after adsorption by $Ag_{1.5}Pd_{1.5}/CeO_2$.

Moreover, once the reaction was conducted at 80 °C over $Ag_{1.5}Pd_{1.5}/CeO_2$ for an hour, the catalyst performance deteriorates irreversibly, and in the following stage at 20 °C the FDCA yield cannot be restored to a level above 20% (Figure. 5.11). The superior catalytic performance of $Ag_{1.5}Pd_{1.5}/CeO_2$ catalyst at 20 °C for the selective oxidation and serious side-reaction at 80 °C result in the product selectivity switch by the reaction temperature.

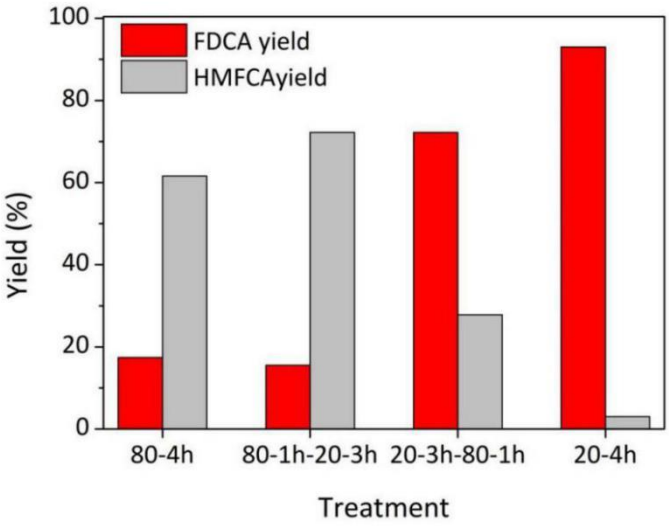

Figure 5.11 The effect of different treatments (temperature and reaction time) on the product selectivity of HMF oxidation. The reactions were conducted in 1 bar O_2 atmosphere, using 3 mL of deionized water mixed with, 0.15 mmol of HMF, 20 mg catalyst and 0.4 mmol NaOH. The total reaction time is 4 h for each treatment.

As the performance of the catalysts depends on the specific surface sites of the metal NPs, transmission electron microscopy (TEM) analysis of a series of catalysts with different Ag:Pd ratios (and thus configurations of surface sites) was conducted. Figure 5.12 shows the results of three alloy catalysts with three Ag:Pd ratios. Panels A-C are TEM bright field images presenting a typical spherical AgPd NPs in about 6 nm diameter (Figure. 5.13) on CeO_2 nanofibres (Figure. 5.14). The spherical morphology of Ag-Pd NPs indicated high index surface nature. The lattice fringes of the nanofibre shown in Figure 5.12D was measured to be 0.31 nm, identical to the *d*-spacing of the plane (111) of FCC CeO_2 structure which lattice parameter a = 0.543 nm. The (111) *d*-spacing for $Ag_{2.5}$ $Pd_{0.5}$ NPs was measured 0.23 nm by using CeO_2 as the scaling reference. This value is slightly larger than that of Pd (111) 0.225 nm but smaller than that of Ag (111) 0.236 nm. This confirmed that the prepared binary nanoparticles are AgPd alloy.

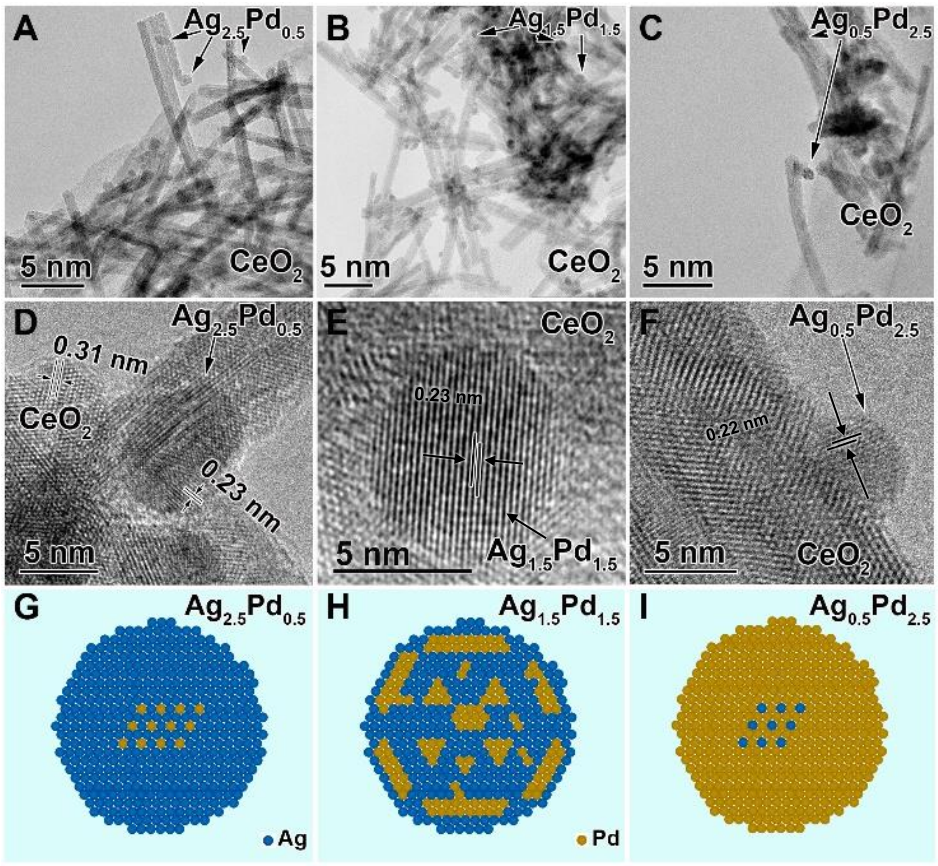

Figure 5.12 TEM analysis of three alloy catalysts with different Ag:Pd ratios. A-C: bright field images; D-F: high resolution TEM micrographs; and G-I: typical atomic configurations of alloy NP surfaces.

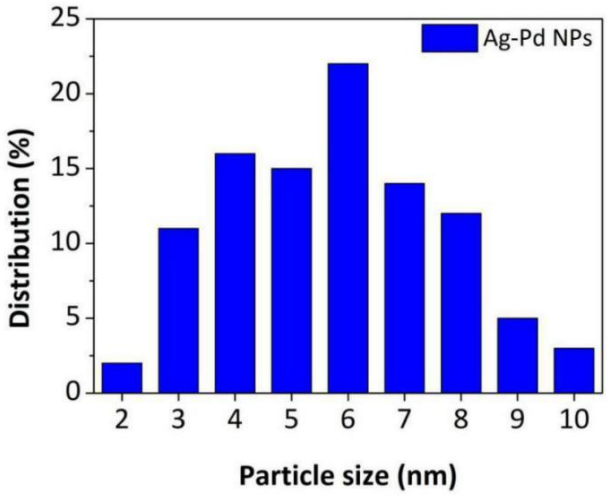

Figure 5.13 Particle size distribution of the Ag-Pd NPs in $Ag_{1.5}Pd_{1.5}/CeO_2$ catalyst determined by measuring over 500 particles in TEM images of the sample.

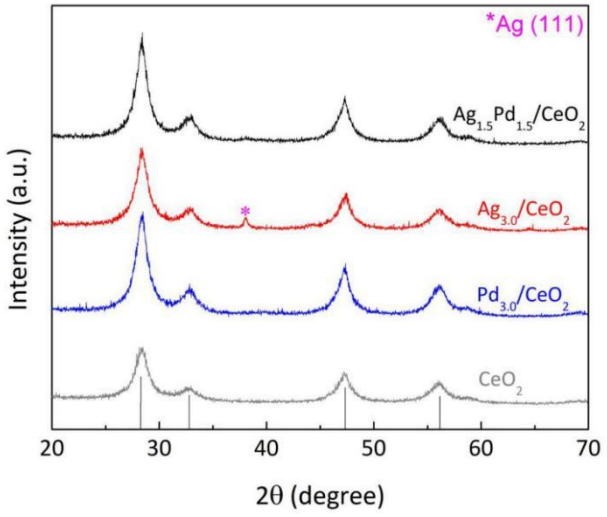

Figure 5.14 XRD patterns of catalysts with $Ag_{1.5}Pd_{1.5}$, $Ag_{3.0}$ and $Pd_{3.0}$ on CeO_2. Vertical bars represent the standard diffraction data for the CeO_2 fibre with a cubic fluorite structure (JCPDS, no. 34-0394).

To identify the atomic configuration at the surface of the AgPd NPs, it is usually in need of atomic resolution scanning electron microscopy and high angle annulate dark field imaging. However, the atomic number contrast of Ag and Pd is very similar to each other because they are neighbour elements in the periodic table. On the other hand, electron energy dispersion (EDS) analysis to the two atoms is also difficult due to the energy Lα of Pd (2.8 eV) being very close to that of Ag (2.9 eV). Therefore, it is much easier to understand the surface atomic configuration of AgPd alloy with different Ag:Pd ratios from energy competition theory. Hoffmann and co-workers

found that AgPd alloy tends to form a short-range ordering pattern when Pd percentage is low but will turn into Pd segregation status when Pd concentration is high (Hoffmann et al., 2016). Yun and co-workers calculated atomic mixing patterns in bimetallic AgPd NPs and suggested a similar result (Yun et al., 2020). With the above reported research outcome, atomic configuration for AgPd NPs studied in this work is schematically shown in Figures 5.12G – I with increasing Pd percentage.

Fig.5.15 shows the catalytic performance of the AgPd alloy catalysts with different Ag:Pd ratios. With this information, we analyse the relationship between the configuration of the surface sites of the alloy NPs and their ability to catalyse reaction steps in the scheme. At an Ag:Pd ratio of 2.5:0.5 ($Ag_{2.5}Pd_{0.5}/CeO_2$), sites of Pd atoms surrounded by Ag atoms exist at facets of the alloy NPs (Figure. 5.12G) as Ag and Pd are infinitely miscible in alloys and the size of Ag atom is similar to that of Pd atom. Such a surface configuration exhibits the best ability to catalyse HMF oxidation yielding HMFCA. As shown in Figure. 5.16, the yield of HMFCA from HMF oxidation within the first hour of reaction gradually decreases when the Ag:Pd ratio further decreases. Hence, the surface configuration of Pd atoms surrounded by Ag atoms is optimal for selectively oxidising carbonyl groups. Nevertheless, this configuration exhibited very limited ability to catalyse the oxidation of HMFCA (Figure. 5.15), especially within the first two hours of reaction (Figure. 5.16).

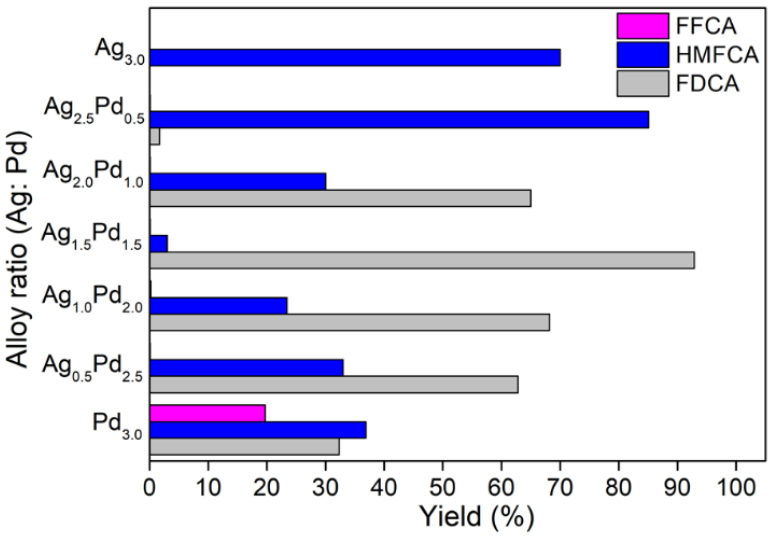

Figure 5.15 Catalytic performance for the oxidation of HMF over Ag−Pd alloy NPs /CeO_2 catalysts with varied composition. Reaction conditions: 0.15 mmol HMF, 20 mg catalyst (with 3 wt% of metals), 0.4 mmol NaOH, 3 mL H_2O, 20 °C for 4 h under a 1 bar oxygen atmosphere.

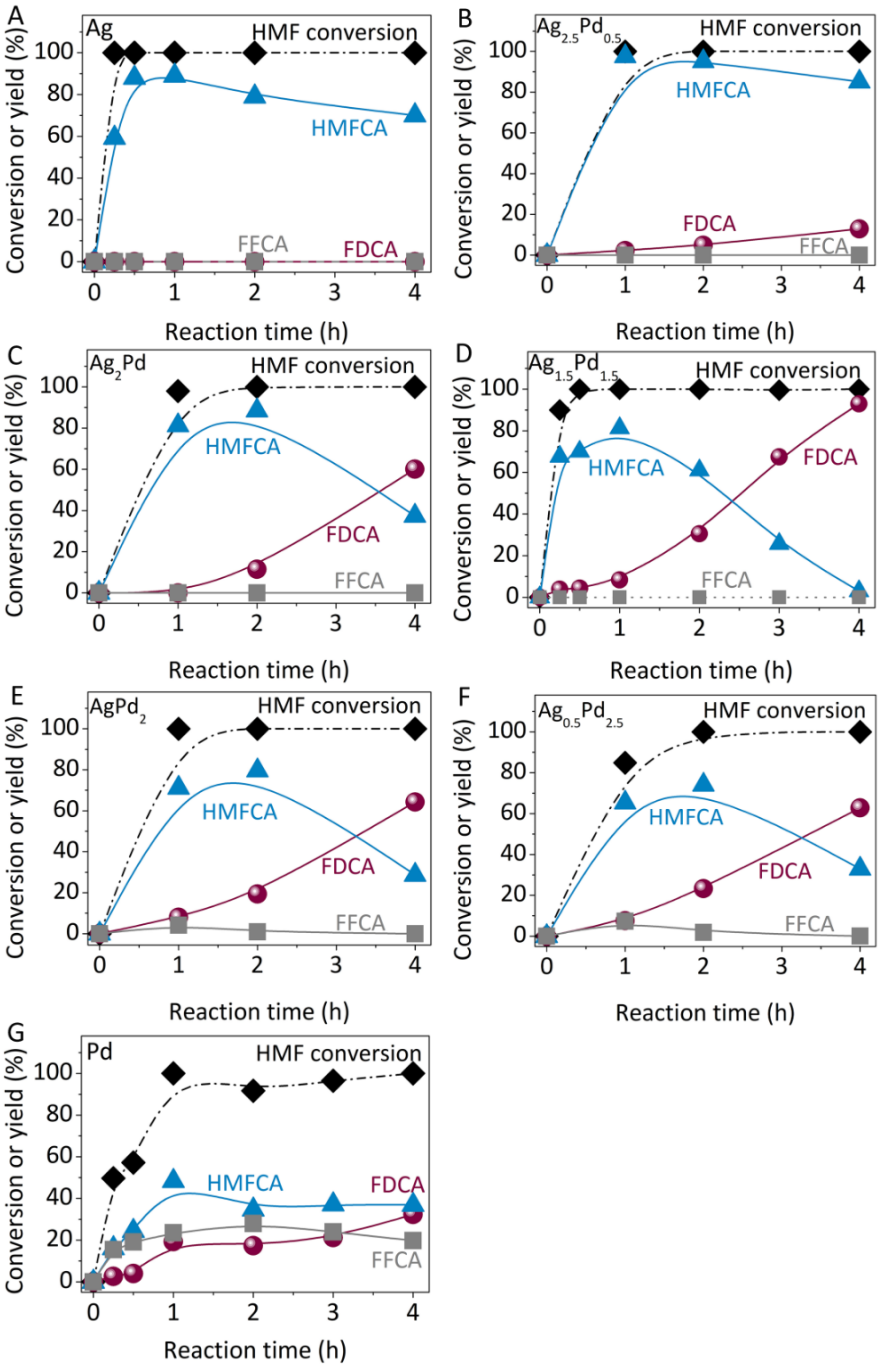

Figure 5.16 Time-course product selectivity of HMF oxidation reaction over Ag3.0/CeO_2 (A), $Ag_{2.5}Pd_{0.5}/CeO_2$(B), $Ag_{2.0}Pd_{1.0}/CeO_2$(C), $Ag_{1.5}Pd_{1.5}/CeO_2$(D), $Ag_{1.0}Pd_{2.0}/CeO_2$(E), $Ag_{0.5}Pd_{2.5}/CeO_2$(F) and $Pd_{3.0}$/CeO2 at 20℃. Reaction condition: HMF (0.15 mmol), catalysts (20 mg, containing 3% of metals), NaOH (0.4 mmol), 3 mL of the solvent H_2O, 20 °C, 4 h under a 1 bar oxygen atmosphere.

The optimal catalytic performance occurs at a ratio of 1.5:1.5. At this ratio, the configuration at the alloy surface is of small Pd clusters that are separated by small Ag

clusters. It appears that the Pd clusters are far more efficient than isolated Pd atoms surrounded by Ag atoms for catalysing the HMFCA oxidation. The segregation by the Ag clusters appears to reduce the occurrence of side-reactions and Ag clusters also exhibit better ability to catalyse the oxidation of carbonyl groups in steps 1 and 3 compared to pure Pd surface in $Pd_{3.0}/CeO_2$ catalyst (Figures. 5.15 and 5.16). This is the optimised configuration for the cascade reaction. Further increases of Pd fraction in the alloy should result in large Pd clusters but reduced ability to catalyse HMFCA oxidation and thus declined FDCA yield is observed (Figure. 5.15). Fig. 5.17 also shows that the catalysts with a lower Ag:Pd ratio exhibit weaker ability to catalyse HMFCA oxidation at 80 °C. The largest mass loss is observed on $Pd_{3.0}/CeO_2$ at 80 °C, and it appears that the large molecule by-products are apt to form on large Pd clusters and Pd surface.

We compared the adsorption energies of reactant, intermediates, and product molecules on the (111) surfaces of Ag, Pd and AgPd (1:1) alloy, which were calculated by PBE method of density functional theory in CP2K code. (Perdew et al., 1996). The detailed parameters of CP2K simulations were listed in Table 5.5. To construct the (111) surfaces of Ag, Pd and Ag-Pd alloy, a 4×4×4 supercell of Ag, Pd and Ag-Pd alloy was optimized first. Then the (111) surfaces were constructed based on the optimized lattices. For Ag and Pd, a (6×6) slab of the (111) surface was constructed, while for Ag-Pd alloy, a (3×6) slab was used. For all as-constructed surface supercells, the lattice parameters *a* and *b* were longer than 16Å, which guarantees the distance between the adsorbed molecules in periodic replica being larger than 9.0Å. Four metal atomic layers were included in the supercells and the lattice parameter c was set to 23Å. When optimizing the structures of the surfaces and the adsorbed molecules, the lattice parameters of the supercells were fixed and the last two metal atomic layers were frozen. An Ag-Pd (111) surface model with an adsorbed HMF molecule was displayed in Figure 5.18. The adsorption energies of the intermediates and product on Pd surface (Table 5.6) are more than 1.74 times of those on AgPd alloy surface. The strong chemical adsorption of the molecules on Pd surface facilitates the side reaction. The adsorption energies on the AgPd alloy surface are about 1.2 times of those on Ag surface, except for 1.46 times for HMF adsorption. The adsorption on the AgPd alloy surface is sufficient to activate the cascade oxidation but cause negligible side-reaction.

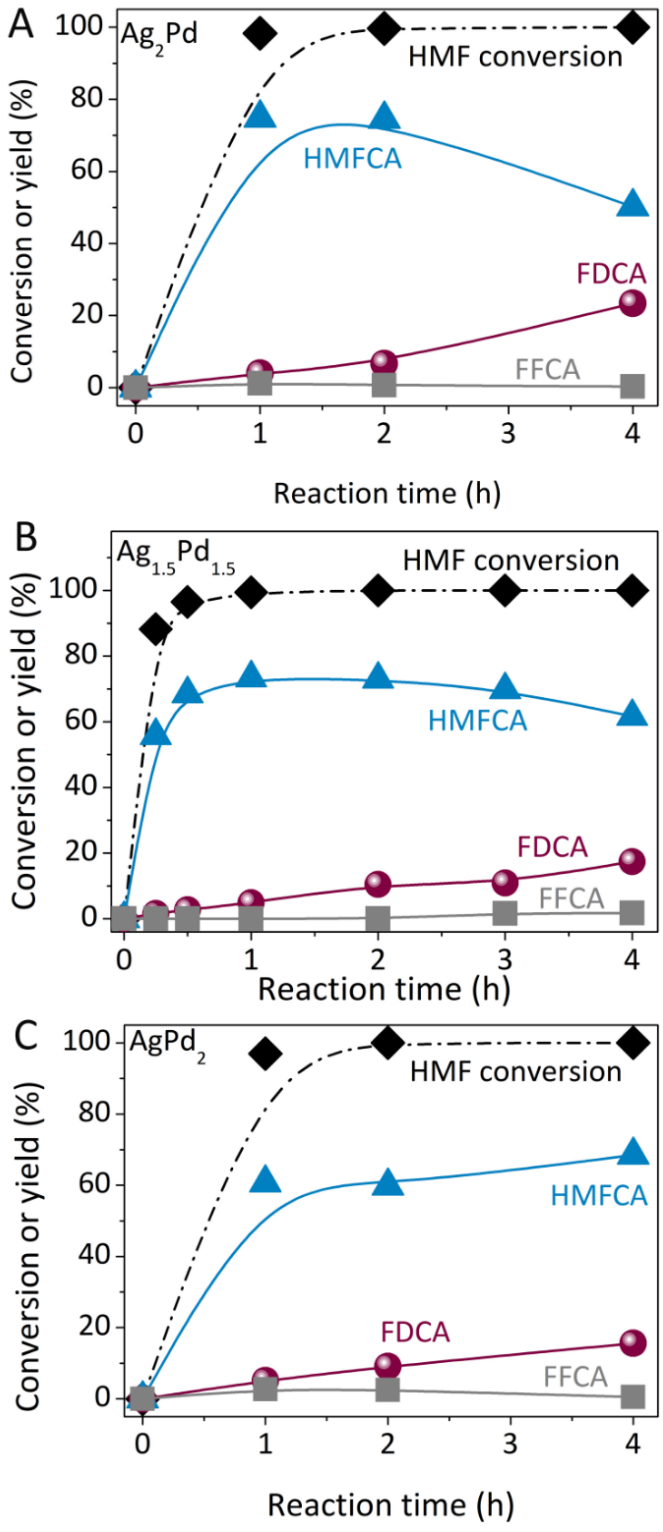

Figure 5.17 Time-course product selectivity of HMF oxidation reaction over $Ag_{2.0}Pd_{1.0}/CeO_2$(A), $Ag_{1.5}Pd_{1.5}/CeO_2$(B) and $Ag_{1.0}Pd_{2.0}/CeO_2$(C) at 80 °C. Reaction condition: HMF (0.15 mmol), catalysts (20 mg, containing 3% of metals), NaOH (0.4 mmol), 3 mL of the solvent H_2O, 80 °C, 4 h under a 1 bar oxygen atmosphere.

Table 5.5 The configurations for the CP2K calculations

Parameter	Value
Method	Mixed Gaussian and Plane-wave (GPW)
Functional	PBE
Dispersive interaction correction	DFT-D3
Pseudo-potential	Goedecker-Teter-Hutter (GTH)
Gaussian-type basis set sets	Molecular optimized double zetha-valence Shorter Range basis sets with a polarization function (DZVP-MOLOPT-SR-GTH)
Plane-wave cut-off	400 Ry
k-point sampling	Gamma-point only
SCF optimizer	Orbital transformation with the direct inverse in the iterative subspace optimizer (OT/DIIS)
Electron density convergence criteria	1.0×10^{-7}
Convergence criteria for geometry optimization	maximum force 4.5×10^{-5} Hartree/Bohr RMS force 3.0×10^{-5} Hartree/Bohr maximum coordinate change 3.0×10^{-4} Bohr RMS coordinate change 1.5×10^{-4} Bohr

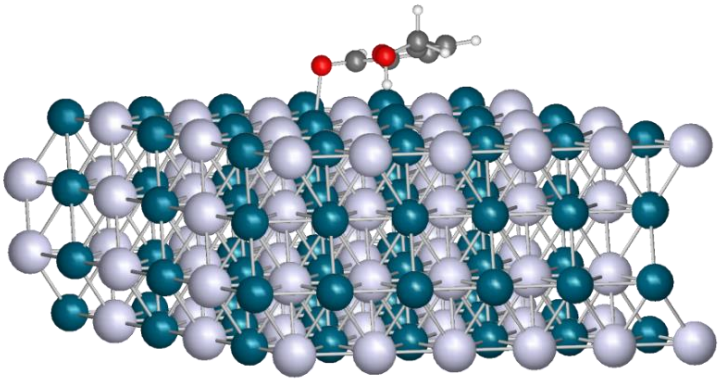

Figure 5.18 The surface model of Ag-Pd (111) with an adsorbed HMF molecule.

Table 5.6 DFT calculations for the adsorptions of HMF, HMFCA, FFCA and FDCA on the (111) surfaces of $Ag_{3.0}$, $Pd_{3.0}$ and $Ag_{1.5}Pd_{1.5}$ alloys

Adsorbate	Adsorption energy ($kJ \cdot mol^{-1}$)		
	$Ag_{3.0}$	$Ag_{1.5}Pd_{1.5}$	$Pd_{3.0}$
HMF	-22.96	-33.49	-47.28
HMFCA	-23.49	-29.56	-51.40
FFCA	-23.94	-28.97	-54.76
FDCA	-24.32	-29.05	-50.61

When the Ag:Pd ratio is 0.5:2.5, sites of isolated Ag atom surrounded by Pd atoms exist at facets of the alloy NPs (Figure. 5.12I). The isolated Ag atom sites have better ability to catalyse the oxidation of carbonyl group of FFCA to yield FDCA than Pd surface in $Pd_{3.0}/CeO_2$ catalyst (Figure. 5.15). Again, a small fraction of one metal alloyed with the other leads to a significant change in the catalytic performance. Furthermore, the FDCA yield achieved by the catalysts with Ag:Pd ratios between 2:1 and 0.5:2.5, are above 70% and higher than that achieved by $Pd_{3.0}/CeO_2$ catalyst. In a wide Ag:Pd ratio range, the alloy catalysts exhibit superior performance to the Pd catalyst. There are Pd clusters dispersed with Ag clusters. These results indicate that the configuration of small Pd clusters segregated by Ag clusters is more efficient than the monometallic Pd surface for selective oxidation of alcohol group to carbonyl group.

5.4 REUSABILITY – RESEARCH OBJECTIVE 4

The possibility of catalyst recycling is a key criterion for heterogeneous catalysts. We carried out a series of experiments to demonstrate the recyclability of Ag1.5Pd1.5/CeO2 catalyst at 20 °C, as shown in Figure. 5.19. The FDCA yield using Ag1.5Pd1.5/CeO2 catalyst maintained 90% without dropping activity considerably for several cycles. Also, it could be found that no obvious morphology and size change were observed from TEM images of AgPd catalysts before and after the reaction.

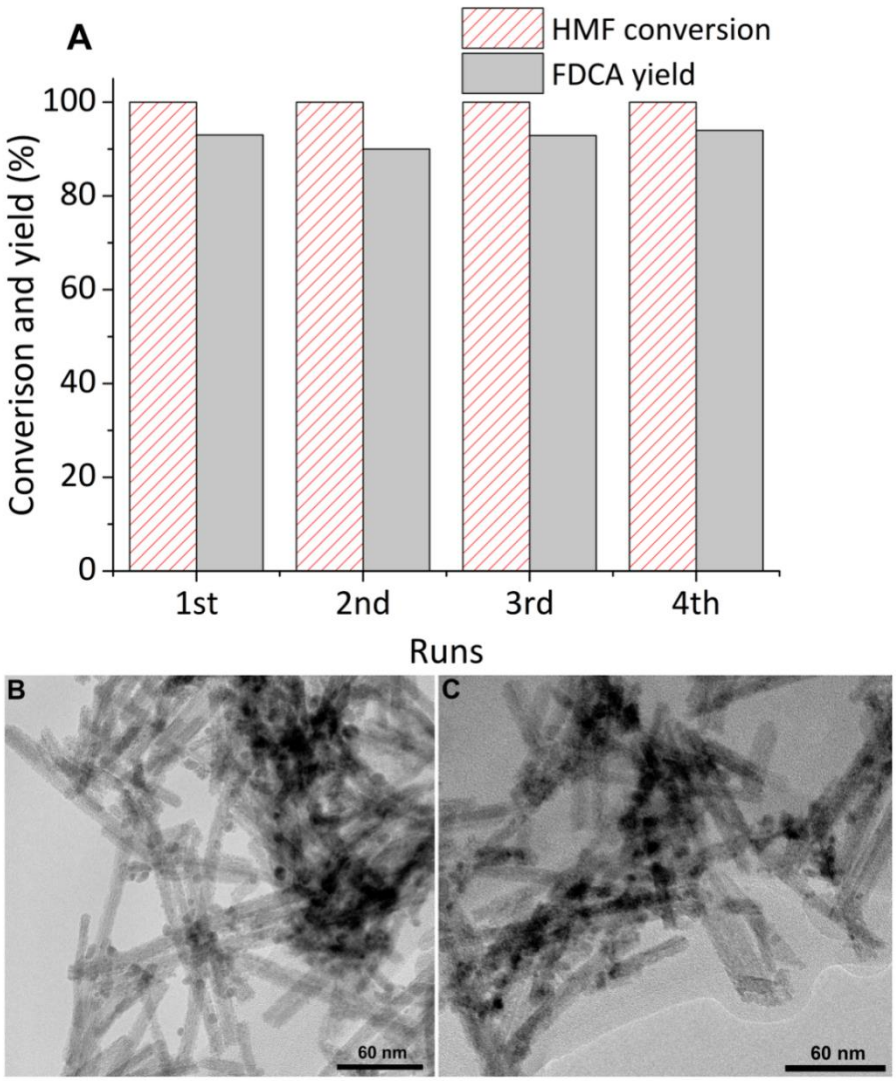

Figure 5.19 Recycling test of $Ag_{1.5}Pd_{1.5}/CeO_2$ for aerobic oxidation of HMF (A). Reaction condition: HMF (0.15 mmol), 20mg catalyst, NaOH (0.4 mmol), 3 mL of the solvent H_2O, 20 °C, 4 h under an oxygen atmosphere, TEM images of (B) $Ag_{1.5}Pd_{1.5}/CeO_2$ catalyst before reaction, (C) $Ag_{1.5}Pd_{1.5}/CeO_2$ catalyst after reaction.

Chapter 6: Conclusions

In summary, this study confirms that the optimal configuration of small Pd clusters segregated by small Ag clusters on the surface of spherical AgPd alloy NPs significantly accelerates the oxidation of both alcohol group to carbonyl group and carbonyl group to carboxyl groups in the selective oxidation of HMF at 20 °C and alleviates formation of large molecule by-products. The adsorption of the reactant, intermediates and product on such surface is suitable to activate the cascade oxidation while avoiding side-reaction. This study found that the side-reaction yielding large by-product takes place on Pd surface sites. The larger the Pd cluster size and the higher temperature are, the more serious the side reaction. The large by-product molecules impede the HMFCA oxidation, the rate-determining step. At 80 °C, the formation of by-products even on $Ag_{1.5}Pd_{1.5}/CeO_2$ are so serious that the oxidation of HMFCA impedes, changing the product selectivity to HMFCA. Thus, it was observed the product selectivity switch with the reaction temperature. This study reveals that the Ag:Pd ratio can be tuned to selectively catalyse the oxidation of the functional groups because the surface configuration of Ag and Pd atoms at the alloys determines the ability to catalyse the functional groups. The knowledge may inspire the design of efficient catalysts for application to the selective oxidation of different functional groups in a wide range of reactants.

Bibliography

Addepally, U., and Thulluri, C. (2015). Recent progress in production of fuel range liquid hydrocarbons from biomass-derived furanics via strategic catalytic routes. *Fuel*, *159*, 935-942.

Alonso, D.M., Bond, J.Q., and Dumesic, J.A. (2010). Catalytic conversion of biomass to biofuels. *Green Chemistry* 12(9)**,** 1493-1513.

Anet, E. F. L. J. (1964). 3-Deoxyglycosuloses (3-deoxyglycosones) and the degradation of carbohydrates. In *Advances in Carbohydrate Chemistry* (Vol. 19, pp. 181-218). Academic Press.

An, J., Sun, G., and Xia, H. (2019). Aerobic oxidation of 5-Hydroxymethylfurfural to high-yield 5-Hydroxymethyl-2-furancarboxylic acid by poly (vinylpyrrolidone)-capped Ag nanoparticle catalysts. *ACS Sustainable Chemistry and Engineering*, *7*(7), 6696-6706.

Ait Rass, H., Essayem, N., and Besson, M. (2015). Selective Aerobic Oxidation of 5-HMF into 2, 5-Furandicarboxylic Acid with Pt Catalysts Supported on TiO_2-and ZrO_2-Based Supports. *ChemSusChem*, *8*(7), 1206-1217.

Bozell, J.J., and Petersen, G.R. (2010). Technology development for the production of biobased products from biorefinery carbohydrates-the US Department of Energy's "Top 10" revisited. *Green Chemistry* 12(4)**,** 539-554.

Cai, J., Ma, H., Zhang, J., Song, Q., Du, Z., Huang, Y., and Xu, J. (2013). Gold nanoclusters confined in a supercage of Y zeolite for aerobic oxidation of HMF under mild conditions. *Chemistry–A European Journal*, *19*(42), 14215-14223.

Caes, B. R., Teixeira, R. E., Knapp, K. G., & Raines, R. T. (2015). Biomass to furanics: renewable routes to chemicals and fuels. *ACS Sustainable Chemistry & Engineering*, *3*(11), 2591-2605.

Casanova, O., Iborra, S., and Corma, A. (2009). Biomass into chemicals: aerobic oxidation of 5-hydroxymethyl-2-furfural into 2, 5-furandicarboxylic acid with gold nanoparticle catalysts. *ChemSusChem: Chemistry and Sustainability Energy and Materials*, 2(12), 1138-1144.

Cha, H. G., and Choi, K. S. (2015). Combined biomass valorization and hydrogen production in a photoelectrochemical cell. *Nature Chemistry*, 7(4), 328.

Chatterjee, M., Ishizaka, T., and Kawanami, H. (2014). Hydrogenation of 5-hydroxymethylfurfural in supercritical carbon dioxide–water: a tunable approach to dimethylfuran selectivity. *Green Chemistry*, *16*(3), 1543-1551.

Corma, A., Iborra, S., and Velty, A. (2007). Chemical routes for the transformation of biomass into chemicals. *Chemical Reviews*, *107*(6), 2411-2502.

Davis, S. E., Houk, L. R., Tamargo, E. C., Datye, A. K., and Davis, R. J. (2011). Oxidation of 5-hydroxymethylfurfural over supported Pt, Pd and Au catalysts. *Catalysis Today*, *160*(1), 55-60.

Davis, S. E., Zope, B. N., and Davis, R. J. (2012). On the mechanism of selective oxidation of 5-hydroxymethylfurfural to 2, 5-furandicarboxylic acid over supported Pt and Au catalysts. *Green chemistry*, 14(1), 143-147.

De Clercq, R., Dusselier, M., and Sels, B. F. (2017). Heterogeneous catalysis for bio-based polyester monomers from cellulosic biomass: advances, challenges and prospects. *Green Chemistry*, *19*(21), 5012-5040.

Delidovich, I., Hausoul, P. J., Deng, L., Pfützenreuter, R., Rose, M., and Palkovits, R. (2016). Alternative monomers based on lignocellulose and their use for polymer production. *Chemical Reviews*, *116*(3), 1540-1599.

Dijkman, W. P., Groothuis, D. E., and Fraaije, M. W. (2014). Enzyme-catalyzed oxidation of 5-hydroxymethylfurfural to furan-2, 5-dicarboxylic acid. *Angewandte Chemie International Edition*, 53(25), 6515-6518.

Elangovan, S., Topf, C., Fischer, S., Jiao, H., Spannenberg, A., Baumann, W., ... and Beller, M. (2016). Selective catalytic hydrogenations of nitriles, ketones, and aldehydes by well-defined manganese pincer complexes. *Journal of the American Chemical Society*, *138*(28), 8809-8814.

Fittig, R., and Heinzelmann, H. (1876). Production of 2, 5-furandicarboxylic acid by the reaction of fuming hydrobromic acid with mucic acid under pressure. *Chem Ber*, 9, 1198.

Gallezot, P. (2012). Conversion of biomass to selected chemical products. *Chemical Society Reviews*, *41*(4), 1538-1558.

Gonis, G., and Amstutz, E. D. (1962). The Preparation of Furan-2, 5-dicarboxylic Acid1. *The Journal of Organic Chemistry*, 27(8), 2946-2947.

Gorbanev, Y. Y., Klitgaard, S. K., Woodley, J. M., Christensen, C. H., and Riisager, A. (2009). Gold-catalyzed aerobic oxidation of 5-hydroxymethylfurfural in water at ambient temperature. *ChemSusChem: Chemistry and Sustainability Energy and Materials*, *2*(7), 672-675.

Goswami, S. R., Dumont, M. J., and Raghavan, V. (2016). Starch to value added biochemicals. *Starch-Stärke*, *3*(68), 274-286.

Hameed, S., Lin, L., Wang, A., and Luo, W. (2020). Recent Developments in Metal-Based Catalysts for the Catalytic Aerobic Oxidation of 5-Hydroxymethyl-Furfural to 2, 5-Furandicarboxylic acid. *Catalysts*, 10(1), 120.

Hanson, S. K., and Baker, R. T. (2015). Knocking on wood: base metal complexes as catalysts for selective oxidation of lignin models and extracts. *Accounts of Chemical Research*, *48*(7), 2037-2048.

Haruta, M., Kobayashi, T., Sano, H., and Yamada, N. (1987). Novel gold catalysts for the oxidation of carbon monoxide at a temperature far below 0 C. *Chemistry Letters*, 16(2), 405-408.

Hayashi, E., Yamaguchi, Y., Kamata, K., Tsunoda, N., Kumagai, Y., Oba, F., and Hara, M. (2019). Effect of MnO_2 crystal structure on aerobic oxidation of 5-hydroxymethylfurfural to 2, 5-furandicarboxylic acid. *Journal of the American Chemical Society*, *141*(2), 890-900.

Hoffmann, M., Marmodoro, A., Ernst, A., Hergert, W., Dahl, J., Lång, J., ... and Kokko, K. (2016). Quantitative description of short-range order and its influence on the electronic structure in Ag-Pd alloys. *Journal of Physics: Condensed Matter*, *28*(30), 305501.

Huang, P. X., Wu, F., Zhu, B. L., Gao, X. P., Zhu, H. Y., Yan, T. Y., ... and Song, D. Y. (2005). CeO_2 nanorods and gold nanocrystals supported on CeO_2 nanorods as catalyst. *The Journal of Physical Chemistry B*, *109*(41), 19169-19174.

Hutchings, G. J. (1985). Vapor phase hydrochlorination of acetylene: Correlation of catalytic activity of supported metal chloride catalysts. *Journal of Catalysis*, 96(1), 292-295.

Jacquel, N., Saint-Loup, R., Pascault, J. P., Rousseau, A., and Fenouillot, F. (2015). Bio-based alternatives in the synthesis of aliphatic–aromatic polyesters dedicated to biodegradable film applications. *Polymer*, *59*, 234-242.

Jadhav, H., Pedersen, C. M., Sølling, T., and Bols, M. (2011). 3-Deoxy-glucosone is an Intermediate in the Formation of Furfurals from D-Glucose. *ChemSusChem*, *4*(8), 1049-1051.

Jang, Y. S., Kim, B., Shin, J. H., Choi, Y. J., Choi, S., Song, C. W., ... and Lee, S. Y. (2012). Bio-based production of C2–C6 platform chemicals. *Biotechnology and Bioengineering*, *109*(10), 2437-2459.

Kang, P. L., Shang, C., and Liu, Z. P. (2019). Glucose to 5-hydroxymethylfurfural: Origin of site-selectivity resolved by machine learning based reaction sampling. *Journal of the American Chemical Society*, *141*(51), 20525-20536.

Kong, X., Zhu, Y., Fang, Z., Kozinski, J. A., Butler, I. S., Xu, L., ... and Wei, X. (2018). Catalytic conversion of 5-hydroxymethylfurfural to some value-added derivatives. *Green Chemistry*, *20*(16), 3657-3682.

Larsen, D. B., Sønderbæk-Jørgensen, R., Duus, J. Ø., and Daugaard, A. E. (2018). Investigation of curing rates of bio-based thiol-ene films from diallyl 2, 5-furandicaboxylate. *European Polymer Journal*, 102, 1-8.

Lei, D., Yu, K., Li, M. R., Wang, Y., Wang, Q., Liu, T., ... and Liu, S. (2017). Facet effect of single-crystalline Pd nanocrystals for aerobic oxidation of 5-hydroxymethyl-2-furfural. *ACS Catalysis*, *7*(1), 421-432.

Lei, L., Wang, Y., Zhang, Z., An, J., and Wang, F. (2020). Transformations of Biomass, Its Derivatives, and Downstream Chemicals over Ceria Catalysts. *ACS Catalysis*, *10*(15), 8788-8814.

Li, C., Zhao, Z. K., Cai, H., Wang, A., and Zhang, T. (2011). Microwave-promoted conversion of concentrated fructose into 5-hydroxymethylfurfural in ionic liquids in the absence of catalysts. *Biomass and Bioenergy*, *35*(5), 2013-2017.

Liu, B., Ren, Y., and Zhang, Z. (2015). Aerobic oxidation of 5-hydroxymethylfurfural into 2, 5-furandicarboxylic acid in water under mild conditions. *Green Chemistry*, *17*(3), 1610-1617.

Mei, N., Liu, B., Zheng, J., Lv, K., Tang, D., and Zhang, Z. (2015). A novel magnetic palladium catalyst for the mild aerobic oxidation of 5-

hydroxymethylfurfural into 2, 5-furandicarboxylic acid in water. *Catalysis Science and Technology*, *5*(6), 3194-3202.

Miao, Z., Wu, T., Li, J., Yi, T., Zhang, Y., and Yang, X. (2015). Aerobic oxidation of 5-hydroxymethylfurfural (HMF) effectively catalysed by a $Ce_{0.8}Bi_{0.2}O_{2-\delta}$ supported Pt catalyst at room temperature. *RSC Advances*.

Mishra, D. K., Lee, H. J., Kim, J., Lee, H. S., Cho, J. K., Suh, Y. W., ... and Kim, Y. J. (2017). $MnCo_2O_4$ spinel supported ruthenium catalyst for air-oxidation of HMF to FDCA under aqueous phase and base-free conditions. *Green Chemistry*, *19*(7), 1619-1623.

Montini, T., Melchionna, M., Monai, M., and Fornasiero, P. (2016). Fundamentals and catalytic applications of CeO_2-based materials. *Chemical Reviews*, *116*(10), 5987-6041.

Morais, A. R., da Costa Lopes, A. M., and Bogel-Łukasik, R. (2015). Carbon dioxide in biomass processing: contributions to the green biorefinery concept. *Chemical reviews*, *115*(1), 3-27.

Moreau, C., Durand, R., Razigade, S., Duhamet, J., Faugeras, P., Rivalier, P., ... and Avignon, G. (1996). Dehydration of fructose to 5-hydroxymethylfurfural over H-mordenites. *Applied Catalysis A: General*, *145*(1-2), 211-224.

Nagarkar, S. S., Chaudhari, A. K., and Ghosh, S. K. (2012). Role of temperature on framework dimensionality: Supramolecular isomers of $Zn_3(RCOO)_8$ based metal organic frameworks. *Crystal growth and design*, 12(2), 572-576.

Nie, J., Xie, J., and Liu, H. (2013). Efficient aerobic oxidation of 5-hydroxymethylfurfural to 2, 5-diformylfuran on supported Ru catalysts. *Journal of catalysis*, *301*, 83-91.

Peiris, E., Sarina, S., Waclawik, E. R., Ayoko, G. A., Han, P., Jia, J., and Zhu, H. Y. (2019). Plasmonic switching of the reaction pathway: Visible-light irradiation varies the reactant concentration at the solid–solution interface of a gold–cobalt catalyst. *Angewandte Chemie International Edition*, *58*(35), 12032-12036.

Perdew, J. P., Burke, K., and Ernzerhof, M. (1996). Generalized gradient approximation made simple. *Physical Review Letters*, *77*(18), 3865.

Pichler, C. M., Al-Shaal, M. G., Gu, D., Joshi, H., Ciptonugroho, W., and Schüth, F. (2018). Ruthenium Supported on High-Surface-Area Zirconia as an Efficient Catalyst for the Base-Free Oxidation of 5-Hydroxymethylfurfural to 2, 5-Furandicarboxylic acid. *ChemSusChem*, *11*(13), 2083-2090.

Rajendran, S., Raghunathan, R., Hevus, I., Krishnan, R., Ugrinov, A., Sibi, M. P., ... and Sivaguru, J. (2015). Inside Back Cover: Programmed Photodegradation of Polymeric/Oligomeric Materials Derived from Renewable Bioresources (Angew. Chem. Int. Ed. 4/2015). *Angewandte Chemie International Edition*, *54*(4), 1369-1369.

Rass, H. A., Essayem, N., and Besson, M. (2013). Selective aqueous phase oxidation of 5-hydroxymethylfurfural to 2, 5-furandicarboxylic acid over Pt/C catalysts:

influence of the base and effect of bismuth promotion. *Green chemistry*, *15*(8), 2240-2251.

Richter, D. T., and Lash, T. D. (1999). Oxidation with dilute aqueous ferric chloride solutions greatly improves yields in the '4+ 1'synthesis of sapphyrins. *Tetrahedron letters*, 40(37), 6735-6738.

Román-Leshkov, Y., Barrett, C. J., Liu, Z. Y., and Dumesic, J. A. (2007). Production of dimethylfuran for liquid fuels from biomass-derived carbohydrates. *Nature*, *447*(7147), 982-985.

Sajid, M., Zhao, X., and Liu, D. (2018). Production of 2, 5-furandicarboxylic acid (FDCA) from 5-hydroxymethylfurfural (HMF): recent progress focusing on the chemical-catalytic routes. *Green Chemistry*, *20*(24), 5427-5453.

Sankar, M., Dimitratos, N., Miedziak, P. J., Wells, P. P., Kiely, C. J., and Hutchings, G. J. (2012). Designing bimetallic catalysts for a green and sustainable future. *Chemical Society Reviews*, *41*(24), 8099-8139.

Sarina, S., Zhu, H., Jaatinen, E., Xiao, Q., Liu, H., Jia, J., ... and Zhao, J. (2013). Enhancing catalytic performance of palladium in gold and palladium alloy nanoparticles for organic synthesis reactions through visible light irradiation at ambient temperatures. *Journal of the American Chemical Society*, *135*(15), 5793-5801.

Siyo, B., Schneider, M., Pohl, M. M., Langer, P., and Steinfeldt, N. (2014). Synthesis, characterization, and application of pvp-pd np in the aerobic oxidation of 5-hydroxymethylfurfural (hmf). *Catalysis Letters*, *144*(3), 498-506.

Siyo, B., Schneider, M., Radnik, J., Pohl, M. M., Langer, P., and Steinfeldt, N. (2014). Influence of support on the aerobic oxidation of HMF into FDCA over preformed Pd nanoparticle based materials. *Applied Catalysis A: General*, *478*, 107-116.

van Es, DSS, Marinkovic, S., Oduber, X., and Estrine, B. (2013). Use of furandicarboxylic acid and its decyl ester as additives in the Fischer's glycosylation of decanol by d-glucose: Physicochemical properties of the surfactant compositions obtained. *Journal of Surfactants Detergents* 16(2), 147-154.

Van Nguyen, C., Liao, Y. T., Kang, T. C., Chen, J. E., Yoshikawa, T., Nakasaka, Y., ... and Wu, K. C. W. (2016). A metal-free, high nitrogen-doped nanoporous graphitic carbon catalyst for an effective aerobic HMF-to-FDCA conversion. *Green Chemistry*, *18*(22), 5957-5961.

Verdeguer, P., Merat, N., and Gaset, A. (1993). Oxydation catalytique du HMF en acide 2, 5-furane dicarboxylique. *Journal of Molecular Catalysis*, *85*(3), 327-344.

Verevkin, S. P., Emel'yanenko, V. N., Stepurko, E. N., Ralys, R. V., Zaitsau, D. H., and Stark, A. (2009). Biomass-derived platform chemicals: thermodynamic studies on the conversion of 5-hydroxymethylfurfural into bulk intermediates. *Industrial and Engineering Chemistry Research*, *48*(22), 10087-10093.

Vinke, P., Van Dam, H. E., and Van Bekkum, H. (1990). New developments in selective oxidation. *Elsevier*, *55*, 147-51.

Wang, M., and Wang, F. (2019). Catalytic Scissoring of Lignin into Aryl Monomers. *Advanced Materials*, *31*(50), 1901866.

Wan, X., Zhou, C., Chen, J., Deng, W., Zhang, Q., Yang, Y., and Wang, Y. (2014). Base-free aerobic oxidation of 5-hydroxymethyl-furfural to 2, 5-furandicarboxylic acid in water catalyzed by functionalized carbon nanotube-supported Au–Pd alloy nanoparticles. *ACS catalysis*, *4*(7), 2175-2185.

Werpy, T., Petersen, G., Aden, A., Bozell, J., Holladay, J., White, J., ... and Jones, S. (2004). Results of screening for potential candidates from sugars and synthesis gas. *Top Value Added Chemicals from Biomass*, 1, 26-28.

Wilsens, C. H., Wullems, N. J., Gubbels, E., Yao, Y., Rastogi, S., and Noordover, B. A. (2015). Synthesis, kinetics, and characterization of bio-based thermosets obtained through polymerization of a 2, 5-furandicarboxylic acid-based bis (2-oxazoline) with sebacic acid. *Polymer Chemistry*, *6*(14), 2707-2716.

Xiao, Q., Sarina, S., Waclawik, E. R., Jia, J., Chang, J., Riches, J. D., ... and Zhu, H. (2016). Alloying gold with copper makes for a highly selective visible-light photocatalyst for the reduction of nitroaromatics to anilines. *ACS Catalysis*, *6*(3), 1744-1753.

Xu, S., Zhou, P., Zhang, Z., Yang, C., Zhang, B., Deng, K., ... and Zhu, H. (2017). Selective oxidation of 5-hydroxymethylfurfural to 2, 5-furandicarboxylic acid using O_2 and a photocatalyst of Co-thioporphyrazine bonded to g-C_3N_4. *Journal of the American Chemical Society*, *139*(41), 14775-14782.

Yi, G., Teong, S. P., and Zhang, Y. (2016). Base-free conversion of 5-hydroxymethylfurfural to 2, 5-furandicarboxylic acid over a Ru/C catalyst. *Green Chemistry*, *18*(4), 979-983.

Yun, K., Nam, H. S., and Kim, S. (2020). Categorization of atomic mixing patterns in bimetallic nanoparticles by the energy competition. *Physical Chemistry Chemical Physics*, *22*(15), 7787-7793.

Zhang, Z., and Deng, K. (2015). Recent advances in the catalytic synthesis of 2, 5-furandicarboxylic acid and its derivatives. *ACS Catalysis*, *5*(11), 6529-6544.

Zhang, Z., Liu, B., Lv, K., Sun, J., and Deng, K. (2014). Aerobic oxidation of biomass derived 5-hydroxymethylfurfural into 5-hydroxymethyl-2-furancarboxylic acid catalyzed by a montmorillonite K-10 clay immobilized molybdenum acetylacetonate complex. *Green Chemistry*, *16*(5), 2762-2770.

Zhang, Z., Zhen, J., Liu, B., Lv, K., and Deng, K. (2015). Selective aerobic oxidation of the biomass-derived precursor 5-hydroxymethylfurfural to 2, 5-furandicarboxylic acid under mild conditions over a magnetic palladium nanocatalyst. *Green Chemistry*, *17*(2), 1308-1317.

Zhao, H., Holladay, J. E., Brown, H., and Zhang, Z. C. (2007). Metal chlorides in ionic liquid solvents convert sugars to 5-hydroxymethylfurfural. *Science*, *316*(5831), 1597-1600.

Zhu, Y., Romain, C., and Williams, C. K. (2016). Sustainable polymers from renewable resources. *Nature*, *540*(7633), 354-362.

Zirbes, L., Nguyen, B. K., de Graaf, D. C., De Meulenaer, B., Reybroeck, W., Haubruge, E., and Saegerman, C. (2013). Hydroxymethylfurfural: a possible emergent cause of honey bee mortality?. *Journal of Agricultural and Food Chemistry*, *61*(49), 11865-11870.